Research Paper

THEMED ISSUE: Different Personalities of Granites and Rhyolites: Silicic Magmas from the Lower Crust to the Surface

GEOSPHERE

GEOSPHERE, v. 18, no. 3

https://doi.org/10.1130/GES02439.1

12 figures; 1 set of supplemental files

CORRESPONDENCE: mpeddy@purdue.edu

CITATION: Eddy, M.P., Pamukçu, A., Schoene, B., Steiner-Leach, T., and Bell, E.A., 2022, Constraints on the timescales and processes that led to high-SiO_2 rhyolite production in the Searchlight pluton, Nevada, USA: Geosphere, v. 18, no. 3, p. 1000–1019, https://doi.org/10.1130/GES02439.1.

Science Editor: Shanaka de Silva
Guest Associate Editor: Guilherme Gualda

Received 2 April 2021
Revision received 22 December 2021
Accepted 11 February 2022

Published online 24 March 2022

Constraints on the timescales and processes that led to high-SiO_2 rhyolite production in the Searchlight pluton, Nevada, USA

Michael P. Eddy[1], Ayla Pamukçu[2], Blair Schoene[3], Travis Steiner-Leach[3], and Elizabeth A. Bell[4]

[1]EAPS Department, Purdue University, West Lafayette, Indiana 47907, USA
[2]Department of Geological Sciences, Stanford University, Stanford, California 94305, USA
[3]Department of Geosciences, Princeton University, Princeton, New Jersey 08544, USA
[4]Earth, Planetary and Space Sciences, University of California, Los Angeles, California 90095, USA

ABSTRACT

Plutons offer an opportunity to study the extended history of magmas at depth. Fully exploiting this record requires the ability to track changes in magmatic plumbing systems as magma intrudes, crystallizes, and/or mixes through time. This task has been difficult in granitoid plutons because of low sampling density, poorly preserved or cryptic intrusive relationships, and the difficulty of identifying plutonic volumes that record the contemporaneous presence of melt. In particular, the difficulty in delineating fossil magma reservoirs has limited our ability to directly test whether or not high-SiO_2 rhyolite is the result of crystal-melt segregation. We present new high-precision U-Pb zircon geochronologic and geochemical data that characterize the Miocene Searchlight pluton in southern Nevada, USA. The data indicate that the pluton was built incrementally over ~1.5 m.y. with some volumes of magma completely crystallizing before subsequent volumes arrived. The largest increment is an ~2.7-km-thick granitic sill that records contemporaneous zircon crystallization, which we interpret to represent a fossil silicic magma reservoir within the greater Searchlight pluton. Whole-rock geochemical data demonstrate that this unit is stratified relative to paleo-vertical, consistent with gravitationally driven separation of high-SiO_2 melt from early-formed crystals at moderate crystallinity. Zircon trace-element compositions suggest that our geochronologic data from this unit record most of the relevant crystallization interval for differentiation and that this process occurred in <150 k.y.

1. INTRODUCTION

High-SiO_2 rhyolite (≥75 wt% SiO_2) is commonly considered to form through differentiation of moderately silicic melts (e.g., dacite) in upper-crustal reservoirs (e.g., Hildreth, 1981; Bachmann and Bergantz, 2004; Lipman and Bachmann, 2015). This process requires the physical separation of early-formed crystals from residual, high-SiO_2 melt and implies that erupted rhyolites are genetically linked to granitoid cumulates. This hypothesis is supported by: (1) phase-equilibria modeling of high-SiO_2 rhyolites, which indicates that they are generated at upper-crustal pressures (≤3 kbar; Gualda and Ghiorso, 2013); (2) geophysical evidence for granitic batholiths beneath many large, silicic volcanic centers (e.g., Lipman and Bachmann, 2015); and (3) an explanation of the compositional Daly gap seen in many volcanic sequences through preferential melt extraction at moderate crystallinity (Dufek and Bachmann, 2010). Nevertheless, global geochemical data sets suggest compositional parity between volcanic and plutonic rocks (Keller et al., 2015; Glazner et al., 2018) and have been used to question whether any granitoids represent cumulates. Additionally, tests of the temporal relationships between high-SiO_2 rhyolites and potential cogenetic plutons have also provided variable evidence for (Deering et al., 2016; Rioux et al., 2016) and against (Mills and Coleman, 2013) a genetic connection. Consequently, the origin of high-SiO_2 rhyolite through upper-crustal differentiation remains questioned (e.g., Lundstrom and Glazner, 2016).

The process of crystal-liquid separation can be tested within an individual pluton through the use of highly incompatible and compatible elements. Highly compatible elements can track accumulation of early-formed crystals, while incompatible elements will track the location of late-stage residual melt. This approach has been used at the regional scale to argue for generation of high-SiO_2 rhyolite through crystal-liquid separation (Lee and Morton, 2015). However, studies that have used a similar approach to document the relative movement of residual melt and early-formed crystals within individual plutons have provided more equivocal results, with some studies finding no evidence for segregation of residual melt (Putnam et al., 2015) and others finding evidence for geochemical stratification (Kamiyama et al., 2007; Hartung et al., 2017; Schaen et al., 2017; Floess et al., 2019; Tavazzani et al., 2020; Schaen et al., 2021). These studies are particularly promising because this information can be used to better evaluate the types of magmatic processes that occur within an individual magma reservoir, as well as the conditions necessary for them to occur.

One challenge to leveraging the plutonic record to study the magmatic processes relevant to volcanism is the difficulty in identifying fossil magma reservoirs, which we define as plutonic volumes that record the coeval presence of melt. Early studies of granitoids frequently treated batholiths as big tank magma chambers (e.g., Bateman and Chappell, 1979). However, improvements

Michael Eddy https://orcid.org/0000-0003-0907-5108

in geochronologic techniques have shown that this interpretation is not applicable over many large-scale intrusive complexes (e.g., Coleman et al., 2004; Matzel et al., 2006; Michel et al., 2008; Memeti et al., 2010; Tappa et al., 2011; Davis et al., 2012; Frazer et al., 2014; Samperton et al., 2015; Shea et al., 2016). Instead, the current view of granitoids is that they are emplaced in discrete increments that can either mix to build increasingly large magma reservoirs or solidify before the next magmatic pulse arrives (e.g., Annen et al., 2015). Much research over the past decade has been focused on modeling the relationship between emplacement rate and magma reservoir size (Annen, 2009; Gelman et al., 2013; Karakas et al., 2017) coupled with geochronologic studies of large batholiths. Yet, a near 1:1 relationship between the number of inferred increments from high-precision geochronologic data and the number of samples analyzed suggests that the sampling density in most plutonic complexes is rarely high enough to identify the vertical or lateral extent of an individual magmatic pulse or an amalgamated magma reservoir (Schoene et al., 2015). There are only a few examples where overlapping high-precision U-Pb zircon crystallization ages have been used to delineate the extent of a possible fossil, silicic magma reservoir (Matzel et al., 2006; Eddy et al., 2016; Rioux et al., 2016; Ratschbacher et al., 2018; Schaen et al., 2021), hindering our ability to use the geometry and geochemistry of these features to study magmatic processes. Here we present a combined geochemical and geochronologic study focused along a single paleo-vertical transect of the Miocene Searchlight pluton in southern Nevada, USA, with sample spacing of ~100 m. The results enable us to identify a fossil silicic magma reservoir within the larger, incrementally assembled intrusive complex, assess its longevity, and use geochemical gradients within the reservoir to explore potential mechanisms for silicic magma differentiation.

2. THE SEARCHLIGHT MAGMATIC SYSTEM

The Miocene Searchlight pluton is exposed in the footwall of the east-dipping Dupont Mountain detachment fault in southern Nevada (Fig. 1). Movement on this fault has exposed a nearly continuous mid- to upper-crustal section of Proterozoic basement, Cretaceous granite, the Miocene Searchlight pluton, and Miocene volcanic and sedimentary rocks (Bachl et al., 2001; Faulds et al., 2001; Zuza et al., 2019). Aluminum-in-hornblende barometry from the Searchlight pluton suggests emplacement pressures ranging from 300 MPa close to the Dupont Mountain detachment fault in the east to 100 MPa in the west. The pressures are consistent with the map distance from the roof of the pluton to each sample, suggesting that the section has been rotated ~90° (Bachl et al., 2001). Detailed geologic mapping of the Searchlight area (1:24,000-scale mapping simplified in Fig. 1) by the Nevada Bureau of Mines provides excellent control on the structural, stratigraphic, and intrusive relationships between rock units in this area.

The Searchlight pluton (SLP) is separated into three map units: (1) an upper unit of quartz monzonite to granite (Upper SLP), (2) a granitic middle unit that includes a capping sill of high-SiO_2 granite (Middle SLP), and (3) a quartz monzonite lower unit (Lower SLP). These units were originally interpreted to represent the upper solidification front, segregated high-SiO_2 melt, and granitic cumulate of a fossil silicic magma chamber, respectively (Bachl et al., 2001). This interpretation is consistent with previously collected whole-rock geochemical data that suggest a common differentiation path for these rocks (Bachl et al., 2001) and geochemical modeling that showed that the compositions are compatible with silicic cumulates and extracted melt (Bachl et al., 2001; Gelman et al., 2014). Nevertheless, these interpretations are in conflict with sensitive high-resolution ion microprobe (SHRIMP) U-Pb zircon data presented in meeting abstracts; these data suggest the magmatic system was emplaced over a period of 1–1.5 m.y. (e.g., Cates et al., 2003; Miller et al., 2006), which would be toward the upper end of modeled melt residence times for upper-crustal, silicic magma reservoirs (Annen, 2009; Gelman et al., 2013; Karakas et al., 2017). The apparent longevity of the system, as inferred from SHRIMP U-Pb zircon geochronology (e.g., Cates et al., 2003; Miller et al., 2006), as well as additional field observations and geochemical measurements, have led to a more nuanced view of the Searchlight pluton that suggests it was incrementally emplaced (e.g., Miller et al., 2006; C. Miller and G. Gualda, 2017, personal commun.). However, the treatment of the Searchlight pluton as a singular fossil magma reservoir has persisted in the literature (Gelman et al., 2014; Bachmann and Huber, 2016). The last major magmatic input into the Searchlight pluton was the intrusion of gabbroic melt into the Middle SLP (Bachl et al., 2001). The gabbro is most voluminous and best exposed in the southern part of the pluton (Fig. 1).

3. METHODS

To better understand the emplacement history of the Searchlight pluton and to identify individual magma reservoirs within it, we dated 117 zircon crystals, or fragments of crystals, from ten samples using chemical abrasion–isotope dilution–thermal ionization mass spectrometry–trace-element analysis (CA-ID-TIMS-TEA) U-Pb zircon geochronology and obtained 79 zircon trace-element analyses via secondary ion mass spectrometry (SIMS), 13 whole-rock major- and trace-element measurements via inductively coupled plasma–optical emission spectroscopy (ICP-OES) and inductively coupled plasma–mass spectrometry (ICP-MS), and 48 whole-rock trace-element measurements made in the field using a portable X-ray fluorescence (pXRF). We focused on a transect parallel to paleo-vertical because many shallow-level plutons are incrementally built by stacked sills (Walker et al., 2007; Michel et al., 2008; Miller et al., 2011; Eddy et al., 2016), and most of the processes proposed for segregating high-SiO_2 rhyolite from upper-crustal magma reservoirs are gravitationally driven (e.g., Bachmann and Bergantz, 2004). The samples from the main transect include both the Lower and Middle SLP. Two additional samples were collected from the Upper SLP in different areas because this unit is not present along the main transect (Fig. 1).

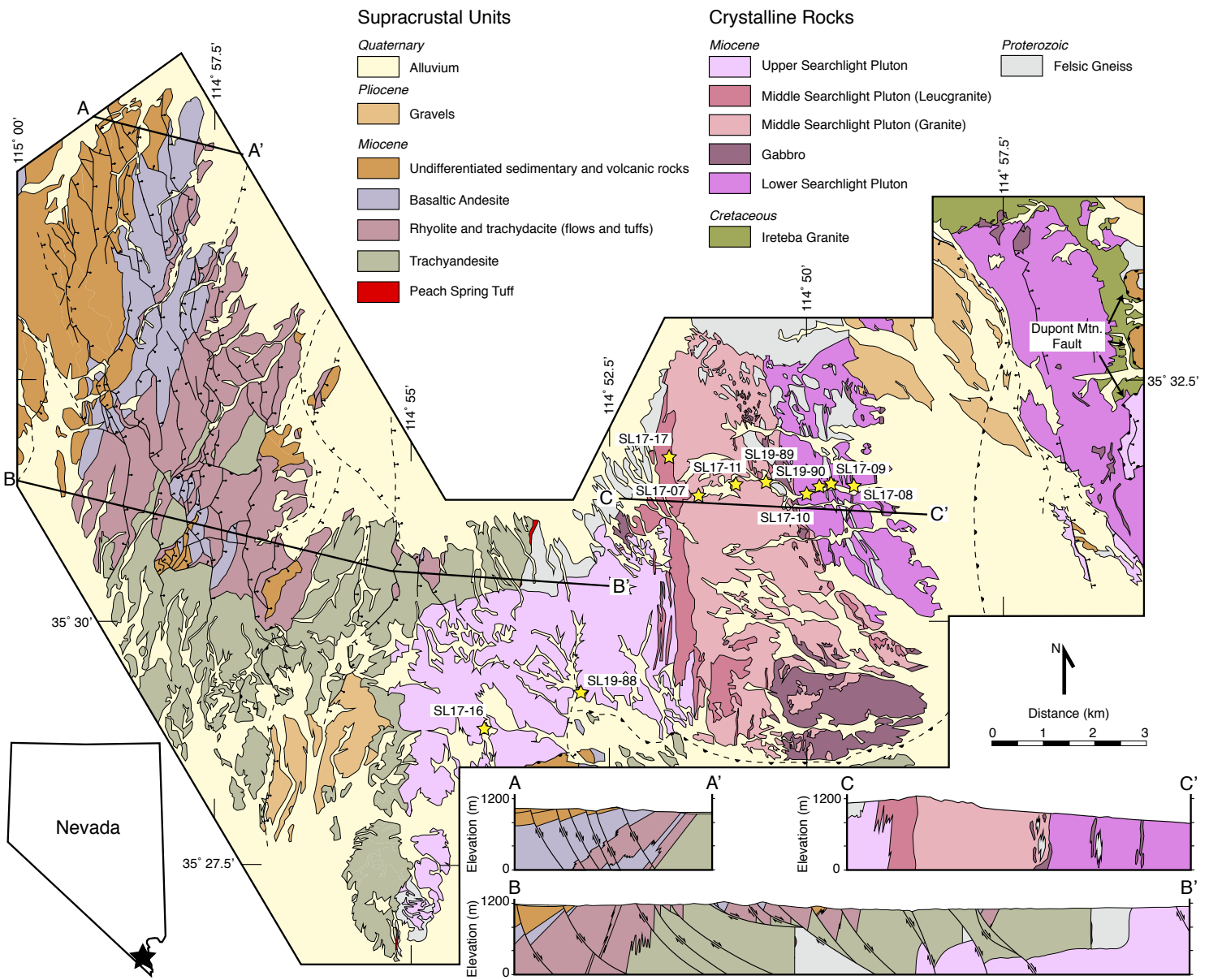

Figure 1. Geologic map and cross sections of the Searchlight magmatic system simplified from Faulds et al. (2002a, 2002b, 2006) and Hinz et al. (2009, 2012). Locations of U-Pb zircon geochronology samples are shown with stars.

3.1 Zircon CA-ID-TIMS U-Pb Geochronology

Individual zircon grains, or fragments of individual zircon grains, were dated from selected samples using U-Pb chemical abrasion–isotope dilution–thermal ionization mass spectrometry (CA-ID-TIMS) geochronology to place high-precision constraints on the timing of magma emplacement, residence, and eruption throughout the Searchlight magmatic system. Zircon crystals were separated from each sample using standard methods and annealed at 900 °C for 60 h. Individual zircon grains, or fragments of zircon grains removed from grain mounts, were then loaded into 200 µl Teflon™ capsules with 100 µl 29 M HF and 25 µl of 30% HNO_3. The capsules were then loaded into a Parr dissolution vessel and held at 215 °C for 12–13 h. This initial digestion is modified from the chemical abrasion method of Mattinson (2005) and is designed to preferentially dissolve parts of the zircon that have accumulated significant radiation damage and may have undergone Pb-loss. After chemical abrasion, the zircon crystals were repeatedly rinsed with clean H_2O, HCl, and HF and spiked with the EARTHTIME ^{205}Pb-^{233}U-^{235}U isotopic tracer (Condon et al., 2015; McLean et al., 2015). The zircon grains were then dissolved in 100 µl of 29 M HF held at 215 °C for 48–60 h. The resulting solutions were dried down and converted to chloride form by dissolving the fluoride salts in 50–75 µl of 6N HCl at 185 °C for ~12 h. After conversion to chloride, the solutions were dried down, dissolved in 75 µl of 3N HCl, and loaded onto 50 µl columns for anion exchange chromatography using AG1-X8 resin and an elution scheme modified from Krogh (1973).

The purified U-Pb aliquots were dried down with 25 µl of 0.5M H_3PO_4 and then loaded onto outgassed, zone-refined rhenium filaments with Merck silica gel. Both Pb and U were analyzed on the IsotopX Phoenix thermal ionization mass spectrometer (TIMS) at Princeton University. Pb was analyzed by peak hopping between ^{204}Pb, ^{205}Pb, ^{206}Pb, ^{207}Pb, and ^{208}Pb on a Daly photomultiplier. Typical beam strengths ranged between 10^1–10^5 kcps for the Pb isotopes, and a Daly dead-time correction of 28.9 ns was used based on runs of the National Bureau of Standards (NBS) 982 Pb isotopic standard at varying intensities. Instrumental fractionation of Pb was corrected using an α of 0.18 ± 0.08 (2σ, %/amu), which represents the average α calculated using the known ratio of $^{202}Pb/^{205}Pb$ in 293 zircon samples run with the EARTHTIME ^{202}Pb-^{205}Pb-^{233}U-^{235}U isotopic tracer (Condon et al., 2015; McLean et al., 2015) at Princeton University. Uranium was measured statically as UO_2 on a set of Faraday detectors, and instrumental mass dependent fractionation was corrected using the average measured $^{233}U/^{235}U$ for each run, the known $^{233}U/^{235}U$ in the EARTHTIME ^{205}Pb-^{233}U-^{235}U isotopic tracer (Condon et al., 2015; McLean et al., 2015), and assuming a zircon $^{238}U/^{235}U$ of 137.818 ± 0.045 (2σ; Hiess et al., 2012). We assume that the measured common Pb (Pb_c) in each analysis is derived from laboratory contamination and does not represent Pb_c incorporated in the zircon grains during crystallization. This assumption is supported by the similarity of Pb_c masses (0.15–1.28 pg) in unknown samples and in procedural blanks. Therefore, we correct for Pb_c using the isotopic composition ($^{206}Pb/^{204}Pb$ = 18.63 ± 0.64, 2σ; $^{207}Pb/^{204}Pb$ = 15.79 ± 0.46, 2σ; $^{208}Pb/^{204}Pb$ = 38.54 ± 0.76, 2σ) of 31 procedural blanks that were run at Princeton University between 2017 and 2019.

A correction for initial secular disequilibrium in the ^{238}U-^{206}Pb decay chain, due to the preferential exclusion of Th relative to U during zircon crystallization, was done using a ratio of Th and U zircon/melt partition coefficients ($f_{ThU} = D_{Th}/D_U$) of f_{ThU} = 0.34 for high-SiO_2 rocks and f_{ThU} = 0.28 for dacites, granodiorite, and monzodiorite. These f_{ThU} values are derived from corresponding zircon rim and glass trace-element analyses from a dacite and high-SiO_2 rhyolite sampled from the Searchlight magmatic system (Claiborne et al., 2018). The resulting ages and isotopic data are presented in Table S1[1]. Some of the dated zircon grains were removed from grain mounts that had been imaged using cathodoluminescence (CL). CL images of these grains are presented in Figure S1.

3.2 Zircon Trace-Element Analyses

The TIMS-TEA (trace-element analysis) approach that we employ here permits the direct measure of the trace-element composition of the same volume of zircon dated by ID-TIMS using solution ICP-MS (Schoene et al., 2010; Samperton et al., 2015). However, some elements are difficult to measure using this method due to low abundance (e.g., Ti). To circumvent this problem, we have used a multi-technique approach to constrain zircon geochemistry, link it to magmatic processes and temperatures, and test the efficacy of the TIMS-TEA method.

In situ trace-element measurements were made using secondary ion mass spectrometry (SIMS) at the University of California at Los Angeles (UCLA). All zircon crystals analyzed by SIMS were first mounted and CL-imaged at Princeton University using a FEI XL30 filament emission gun (FEG) scanning electron microscope (SEM) with a Gatan miniCL detector. Analyses of Ti, Y, REE, Hf, Th, and U were conducted at UCLA using a CAMECA ims1270 ion microprobe using a 15 nA O-primary beam focused to ~30 µm to generate secondary ions, with a –100V energy offset to suppress molecular interferences (e.g., Bell et al., 2016). Instrumental mass fractionation and relative sensitivity factors were determined using repeat analyses of the National Institute of Standards and Technology (NIST) 610 glass, and peak stripping for remaining isobaric interferences was done offline. A secondary correction for Ti measurements was done using repeat measurements of the 91500 zircon reference material (Wiedenbeck et al., 2004). The location of each analysis is presented in Figure S1 (footnote 1). Analyses were screened to ensure that they represent zircon and were excluded if there was evidence for the analysis incorporating an inclusion via: (1) visual evidence from the CL image; (2) a chondrite-normalized REE pattern that deviates significantly from that expected in zircon (e.g., Hoskin and Schaltegger, 2003); or (3) clear enrichment in Ti beyond what is normally observed in zircon (i.e., Harrison et al., 2007). The resulting data set is presented in Table S2 (footnote 1), and CL images of the analyzed zircon grains are presented in Figure S1.

[1]Supplemental Material. Figures and tables. Please visit https://doi.org/10.1130/GEOS.S.19163798 to access the supplemental material, and contact editing@geosociety.org with any questions.

We utilized the TIMS-TEA method (Schoene et al., 2010; Samperton et al., 2015) to measure the trace-element composition of the same volume of zircon analyzed for U-Pb CA-ID-TIMS geochronology. These measurements were made at Princeton University on the wash solution produced during anion exchange column chemistry used to separate U and Pb for CA-ID-TIMS geochronology, because this solution contains the trace-element content of the dissolved zircon. This wash solution was collected, dried down, and converted to 1 ml 3% HNO_3 + 0.2% HF + 1 ppb In. It was then measured on a Thermo-Fisher iCAP quadrupole ICP-MS using a Teledyne-Cetac ASX-100 autosampler. Measured elements include Zr, Hf, Sc, Y, Nb, Ta, REE, and In (used as an internal standard). A dilution series of a synthetic zircon solution was used to generate a concentration-intensity calibration curve over the range of concentrations observed in most zircon TIMS-TEA analyses. Reproducibility was assessed using a homogeneous solution of Plešovice zircon (Sláma et al., 2008) and a solution with known Zr and Hf concentrations. Measurements of procedural blanks were monitored for laboratory trace-element contamination. Unknowns, procedural blanks, and the standard Plešovice solution were run in batches of 30 before a new concentration-intensity curve was generated. Between each analysis, the autosampler was rinsed and flushed with 3% HNO_3 + 0.2% HF for 60 s to ensure that there was no contamination between samples. Solution measurements were converted to zircon concentrations by assuming that all of the measured trace elements substitute for Zr^{4+}, such that Σ = Zr + Hf + Sc + Y + Nb + Ta + REE = 497,646 ppm. The results from the analyses are presented in Table S1. Procedural blanks show no significant laboratory trace-element contamination. Repeat runs of the Plešovice zircon solution show good reproducibility for rare-earth elements heavier than Nd (Fig. S2 [footnote 1]).

3.3 Whole-Rock Geochemistry

Samples selected for whole-rock major- and trace-element analyses were first trimmed to remove weathered portions and sanded to remove saw marks. Aliquots with masses between 1 and 2 kg were then sent to a commercial geochemical laboratory (Activation Laboratories Ltd. in Ancaster, Ontario, Canada) for crushing, rotary splitting, and powdering. Five grams of the resulting homogenous powder were fused using a mixture of lithium metaborate and lithium tetraborate and dissolved in 5% HNO_3 containing an internal standard. Major elements were analyzed by solution ICP-OES on either a Thermo Jarrell-Ash ENVIRO II ICP or a Varian Vista 735 ICP and calibrated using certified reference materials. Trace elements were analyzed from the solution using a Perkin Elmer Sciex ELAN 6000, 6100, or 9000 ICP-MS. The results of these whole-rock analyses are presented in Table S3.

Additional whole-rock trace-element measurements were made in the field using the factory-calibrated SciApps Soil application on a SciApps X350 pXRF. X-rays were generated using an Au anode operating for 20 s at 50 kV for Ba and 20 s at 40 kV for Rb and Sr. The analyzed area for each sample is ~8 mm in diameter with a penetration depth of <1 cm. To account for the small analysis area relative to the grain size in the Searchlight samples, we averaged 25 measurements from randomly selected spots for each unknown. In heterogeneous materials, such as coarse-grained granitoids, we do not expect the distribution of results to be Gaussian and therefore calculated the concentration and associated uncertainty using 10^4 unweighted bootstrap means. In the few samples where concentrations of the desired elements were extremely low and could not be measured, we used 0.5 of the reported detection limits.

The pXRF measurements were made under different environmental conditions over the course of many days. To monitor and correct for instrumental drift, we analyzed the same granitic powder before each sample and applied a linear correction factor to the unknown. Variation in the analyses included periods that could be attributed to analytical scatter (e.g., Rb on field day 4; Fig. 2) and periods that seem to show secular drift of up to ~10% over a few hours (e.g., Sr and Ba on field day 3; Fig. 2). Future studies using this method should carefully evaluate whether this correction is beneficial. However, we applied it to the data collected in this study given the periods of apparent secular drift. A final, empirical correction for matrix effects and/or the effects of analyzing irregular surfaces was done by calibrating our results relative to hand samples with known elemental concentrations. The calibration curves are linear (Fig. 3) and provide a simple correction for these effects. Long-term reproducibility can be assessed using analyses of hand sample SL17-08, which were completed throughout the study and demonstrate that our approach reproduces the concentration of Rb, Sr, and Ba to within ~10% of the reference values (Fig. 4). The importance of the drift and empirical correction can be assessed using Figure 4. The effect of the drift correction is variable. The empirical correction for matrix effects does not make a significant difference in the results for Rb and Ba but significantly improves the accuracy of the measured Sr concentrations. This relationship is due to the pXRF consistently underestimating Sr concentrations (Fig. 3). The results of the pXRF study are reported in Table S4 (footnote 1).

4. RESULTS

4.1 Zircon U-Pb Geochronology

Our U-Pb zircon geochronology is shown in Figure 5 as a rank-order plot of $^{206}Pb/^{238}U$ dates as well as a probability density plot using all of the dated zircon grains from the Lower, Middle, and Upper SLP. The data set spans ~1.5 m.y. and is in a good agreement with the duration of pluton construction as inferred from U-Pb zircon SHRIMP dates (Cates et al., 2003; Miller et al., 2006), but the higher precision on our dates permits us to interrogate intra- and inter-sample age dispersion at a higher resolution. Collectively, samples from the Lower and Upper SLP contain zircon grains that crystallized between ca. 17.50 and 16.25 Ma (Fig. 5A). However, no single sample contains zircon dates that span

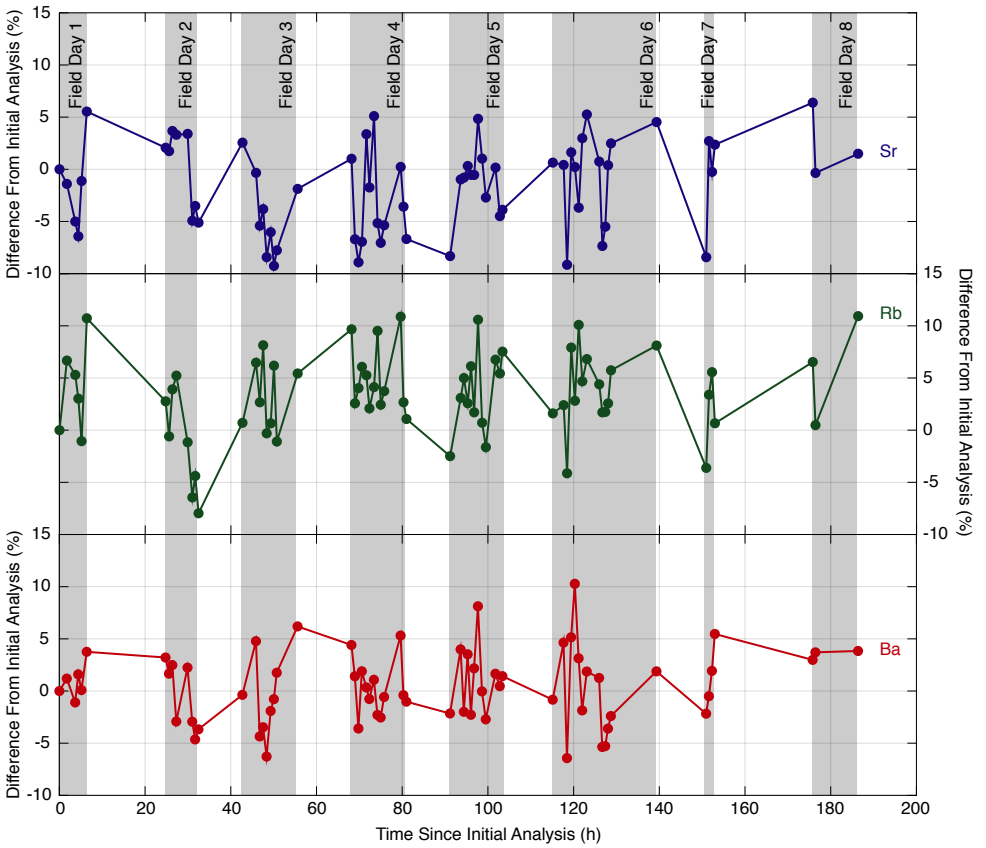

Figure 2. Concentrations of Sr, Rb, and Ba determined using portable X-ray fluorescence (pXRF) on a homogenous granitic powder that was repeatedly analyzed over the course of the study. The results are shown as a percent difference from the initial analysis. This powder was analyzed prior to every unknown in order to provide a drift correction and shows variation of up to ~15% over the course of a single field day (shown as vertical gray bars). Some periods of time show secular changes that are consistent with instrumental drift (e.g., field day 2 for Sr and Ba) and other periods show variation that is more consistent with analytical scatter (e.g., field day 4 for Rb).

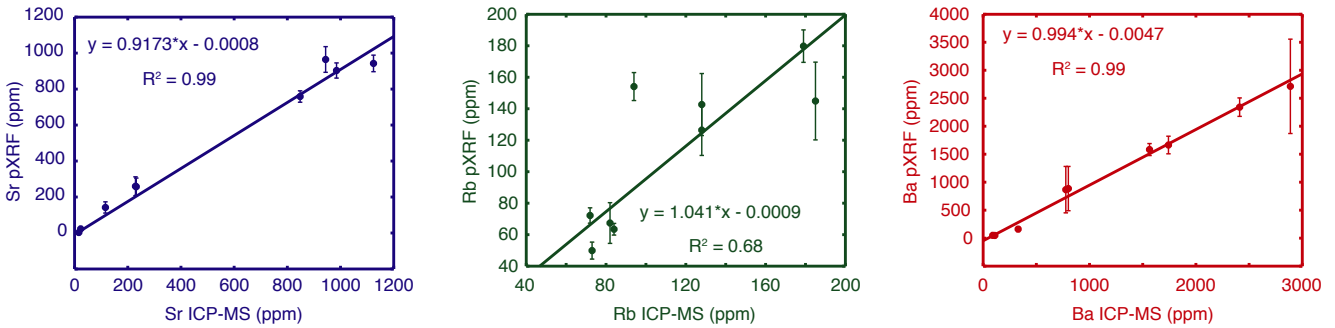

Figure 3. Empirical calibration curves between portable X-ray fluorescence (pXRF) output using drift-corrected results from the factory-built soil mode calibration and inductively coupled plasma mass spectrometry (ICP-MS) data from the same samples. The linear relationships were used to correct for any systematic bias in the pXRF data that might arise from matrix effects for unknowns without accompanying ICP-MS data.

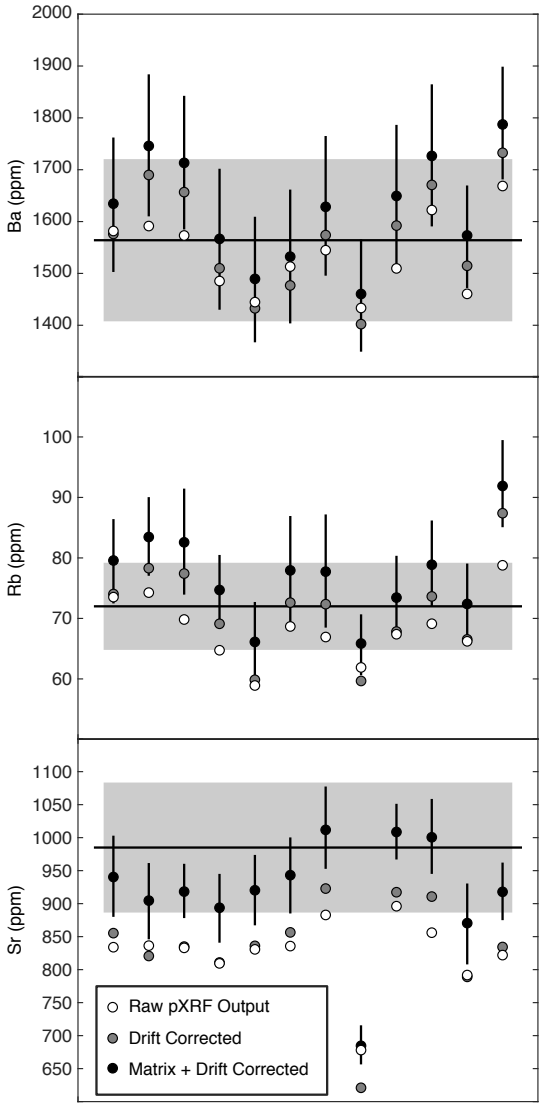

Figure 4. Reproducibility of portable X-ray fluorescence (pXRF) measurements of Sr, Rb, and Ba from a single hand sample (SL17-08) that was repeatedly measured over the course of the study. The black lines represent the reference values for these elements as determined by inductively coupled plasma mass spectrometry (ICP-MS) and the gray box represents 10% deviation from these reference values. Raw output from the pXRF is shown as white circles, concentrations from drift-corrected data are shown as gray circles, and data corrected for both drift and matrix effects are shown as black circles with the full associated uncertainty. Most of our corrected measurements are within 10% of the reference value, giving us confidence in our approach to using the pXRF on coarse-grained granitoids.

that full range. All four samples from the Middle SLP yield zircon $^{206}Pb/^{238}U$ dates between 16.25 and 16.10 Ma with two outliers from the Middle SLP leucogranite (SL17-17: Fig. 5A) that are several 100 k.y. older. We interpret these outliers to be recycled from older parts of the magmatic system and ignore them in our subsequent discussion of the duration of zircon crystallization.

Most of the dated samples show minor age dispersion beyond what is expected from analytical uncertainty. Age dispersion is increasingly recognized in high-precision U-Pb zircon geochronology (e.g., Rioux et al., 2012; Schoene et al., 2012; Wotzlaw et al., 2013; Samperton et al., 2015) and can represent analytical uncertainties that are underestimated or age dispersion of geological significance. We rule out the former possibility because natural and synthetic zircon reference materials are reproducible to within 0.03%–0.10% in the Princeton University geochronology lab (Eddy et al., 2019; Schoene et al., 2019) and discuss the potential geological sources of age dispersion in our samples in section 5.2.

To quantify the age dispersion within each sample, we randomly sampled the Gaussian uncertainty interval of a sample's oldest and youngest grains and found the absolute value of the difference. This approach is functionally the same as finding the difference between the oldest and youngest grain. However, random sampling and imposing the constraint of a positive age difference help quantify the duration and its associated uncertainty when the two dates have overlapping analytical uncertainties. The results of this analysis are shown in Figure 5B and show that the dated zircon grains from most samples record 100–150 k.y. of resolvable age dispersion, with the exception of SL17-6 from the Upper Searchlight pluton, which shows up to 300 k.y. of age dispersion, and the high-SiO_2 leucogranite of the Middle SLP (SL17-17), which shows <100 k.y. of age dispersion (Fig. 5B).

4.2 Zircon Trace-Element Analyses

Figure 6 shows trace-element cross plots comparing SIMS and TIMS-TEA zircon trace-element data for several indices of magmatic differentiation: Eu/Eu* as a record of feldspar crystallization, Dy/Yb as a record of amphibole or titanite crystallization, Ti as a proxy for temperature in zircon (Ferry and Watson, 2007), and Hf concentration as an index of magma differentiation (Claiborne et al., 2006). All of these relationships are well understood, and their general relationship with time can be predicted a priori for simple closed-system crystallization behavior. However, more complex open-system behavior, such as magma mixing, thermal perturbations due to injection of new magma, or convective mixing of crystals from different parts of the magma reservoir, will complicate these relationships. Zircon compositions from the Middle SLP correspond to the expected trends for a differentiating magma with negative covariance between Hf and Dy_{CN}/Yb_{CN}, Eu/Eu*, and Ti (Fig. 6). Zircon compositions from the Lower and Upper SLP show the same relationships. However, they do not record a coherent relationship between Hf and Eu/Eu*. Overall, the SIMS and TIMS-TEA measurements show the

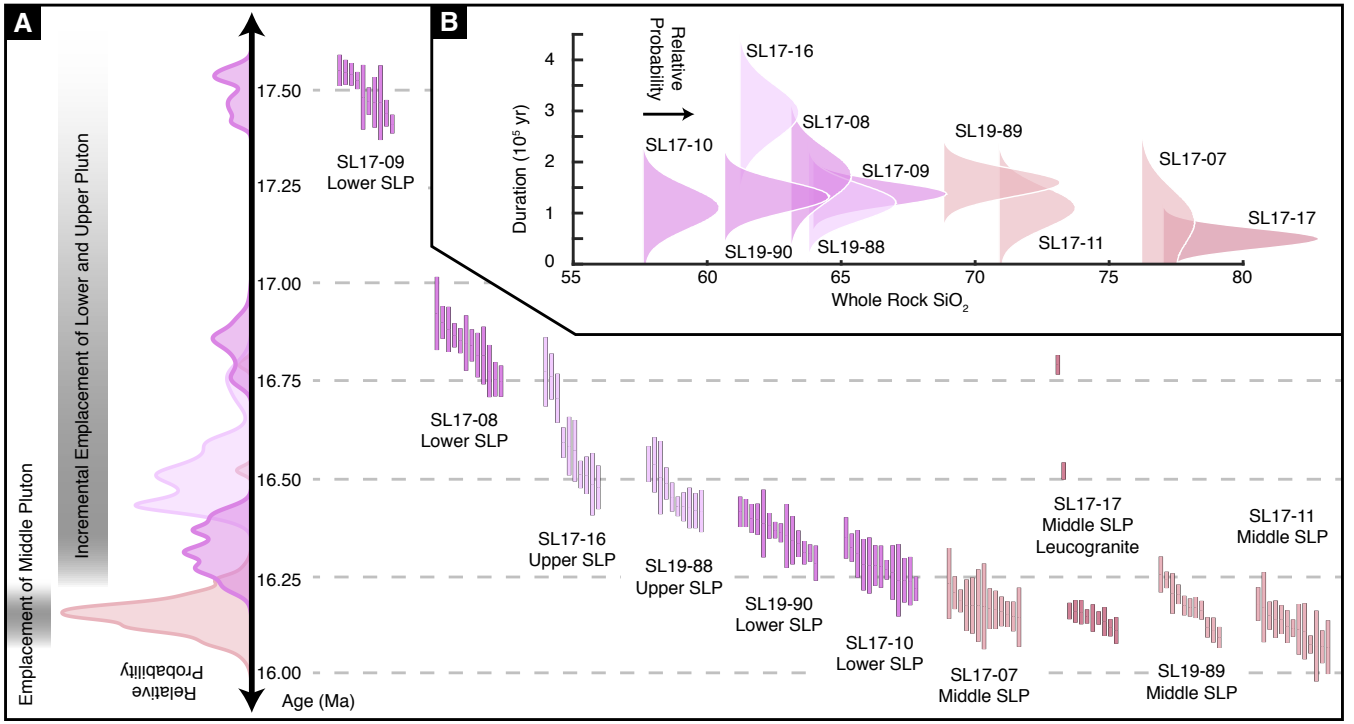

Figure 5. (A) Rank order plot of all zircon dated by chemical abrasion–isotope dilution–thermal ionization mass spectrometry (CA-ID-TIMS) U-Pb zircon geochronology as part of this study and a probability density plot of the same data. We interpret the age distributions to suggest incremental emplacement of the Upper and Lower Searchlight pluton with little to no communication between different increments. The Middle Searchlight pluton shows substantial overlap and is interpreted to represent a fossil magma reservoir. (B) Estimates for the duration of zircon crystallization in each sample derived from 10^7 Monte Carlo draws from the oldest and youngest zircon in each sample and finding the age difference.

same range of elemental concentrations. However, the SIMS measurements extend to compositions expected to crystallize from more evolved magma (lower Eu/Eu*, lower Dy_{CN}/Yb_{CN}, lower Ti, and higher Hf), which is likely a consequence of the fact that TIMS-TEA analyses integrate a larger volume from each grain.

One advantage of the TIMS-TEA approach is that geochemical measurements can be paired with high-precision U-Pb dates. Figure 7 shows $^{206}Pb/^{238}U$ dates plotted relative to Eu/Eu*, Dy/Yb, and Hf for selected samples, and the same plots for all of the dated samples are presented in Figure S3. Some samples show simple relationships that are compatible with monotonic cooling (e.g., SL19-89: Fig. 7), but many show no clear geochemical trends with time (e.g., SL17-07; Fig. 7) or trends opposite of those expected for a monotonically cooling magma reservoir (e.g., SL17-09; Fig. 7). We discuss the potential reasons for these differences in section 5.2.

4.3 Whole-Rock Geochemistry

Our whole-rock geochemical data are presented in Tables S3 and S4 (footnote 1) and shown in Figure 8. The dated samples span the full compositional range of granitoids within the Searchlight pluton, with the exception of the highest SiO_2 end-member compositions for the Lower and Upper SLP (Fig. 8). Compositions of the Middle SLP plot as a linear array on the quartz-albite-orthoclase (Qz-Ab-Or) ternary with one end of the array terminating near the 0.1 GPa H_2O-saturated minimum and trending toward the Ab-Or join (Fig. 9). The array shows some scatter between our data and the data from Bachl et al. (2001). However, the data from our sampling transect is linear and has a clear relationship between each sample's composition and its depth below the roof of the pluton. Samples at the top of the Middle SLP plot on the 0.1 GPa minimum, and samples from deeper in the section plot progressively closer to the Ab-Or join (Fig. 9).

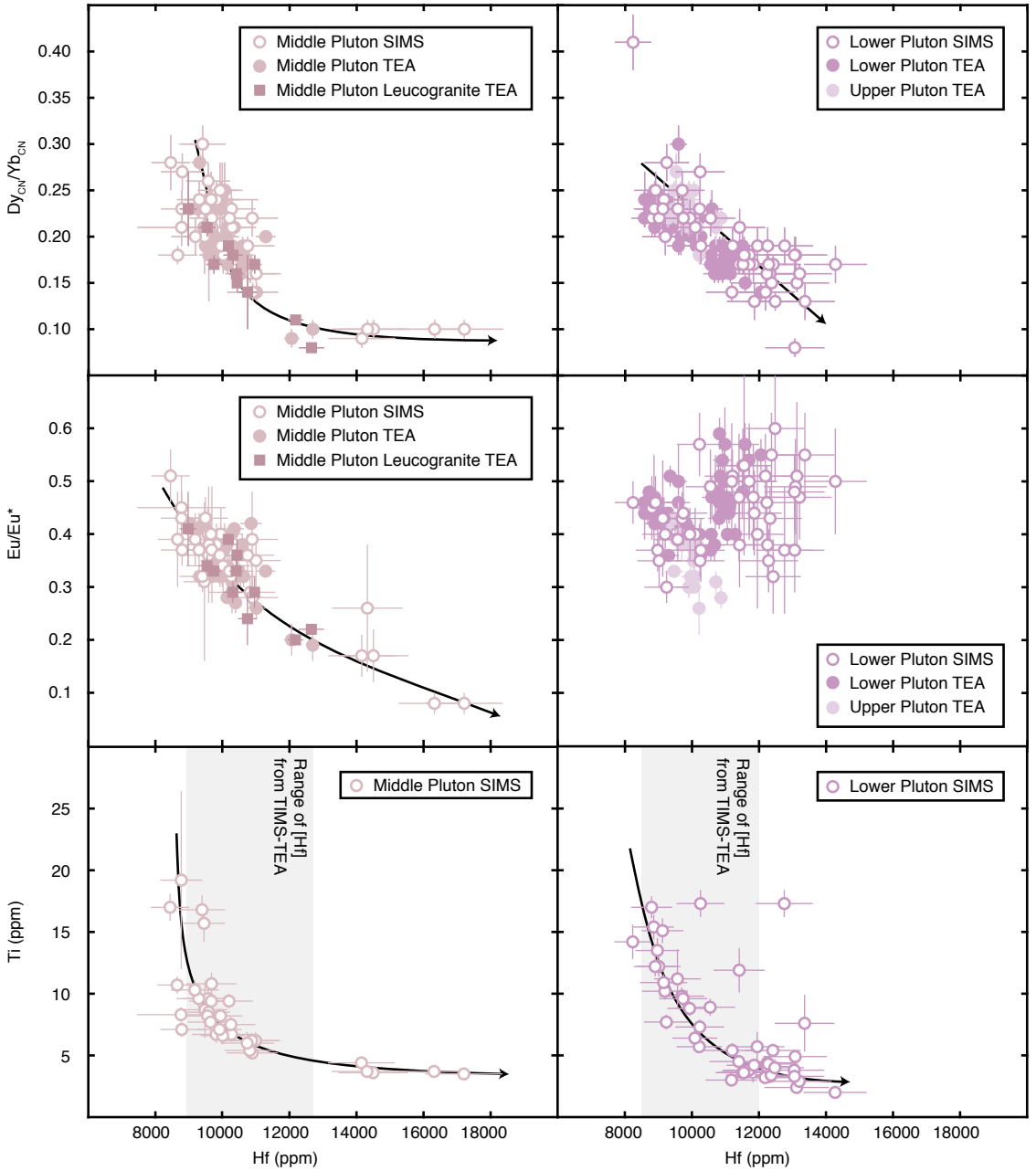

Figure 6. Comparison of zircon Dy_{CN}/Yb_{CN}, Eu/Eu*, and Hf compositions measured by secondary ion mass spectrometry (SIMS) and thermal ionization mass spectrometry–trace-element analysis (TIMS-TEA) as part of this study. Despite integrating much larger volumes of zircon, the TIMS-TEA data encompass most, but not all, of the values seen in the SIMS data (see text for discussion of this limitation). Plots of Ti versus Hf are also shown. Ti-in-zircon scales with temperature (Ferry and Watson, 2007) and Hf-in-zircon generally increases with increased magma differentiation (Claiborne et al., 2006; Colombini et al., 2011). Comparing the range of Hf concentrations measured via TIMS-TEA to the paired Hf-Ti concentrations measured by SIMS suggests that the TIMS-TEA data records all but the lowest temperature evolution of these magmas.

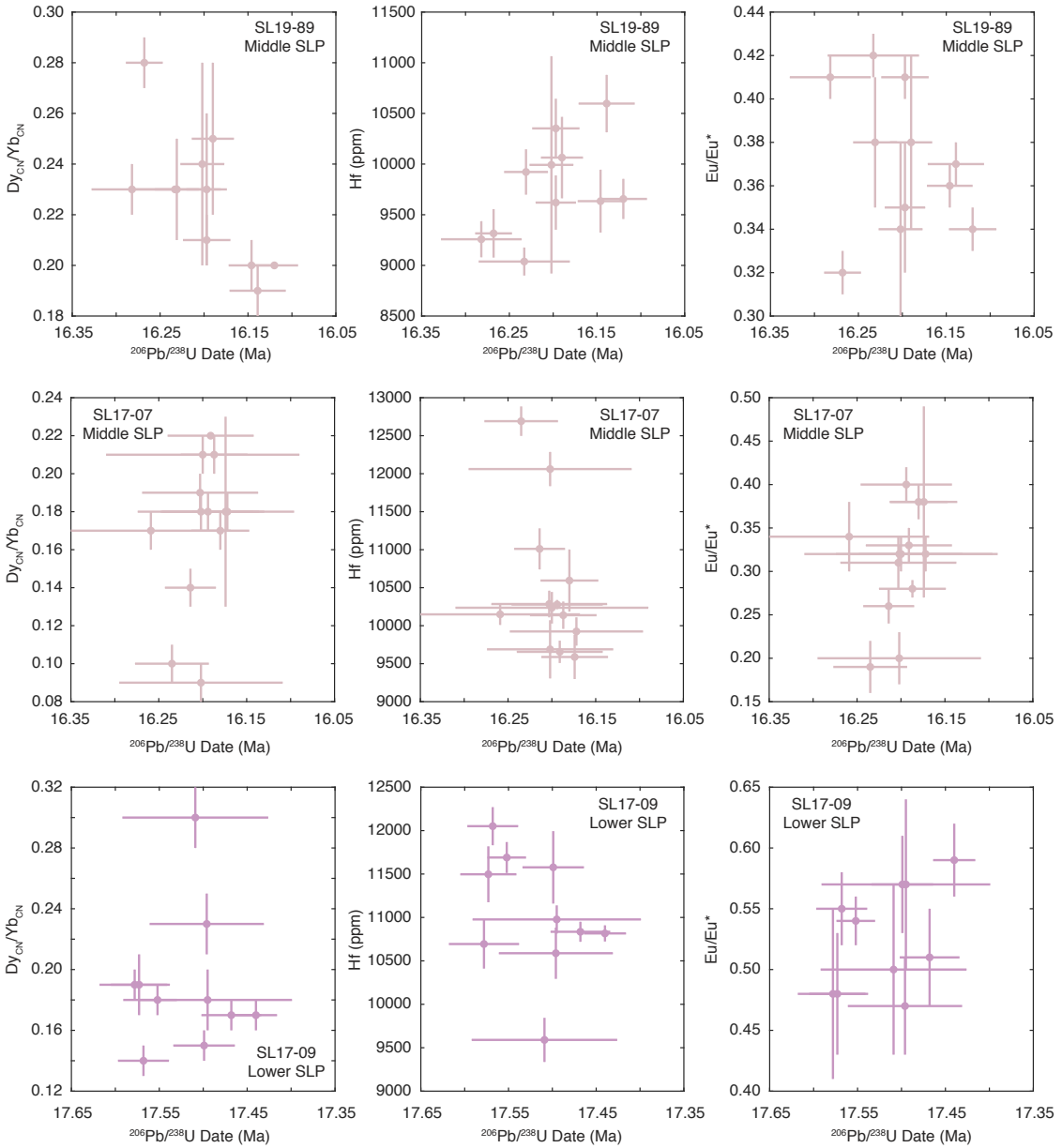

Figure 7. Selected plots of samples showing the expected relationships between zircon geochemistry and time (SL19-89), no relationship between zircon geochemistry and time (SL17-07), and unexpected relationships between zircon geochemistry and time (SL17-09) in our thermal ionization mass spectrometry–trace-element analysis (TIMS-TEA) data set. The lack of a relationship between chemistry and time in SL17-07 can be reconciled by noting there is little resolvable age dispersion in this sample. The unpredicted results in SL17-09 are attributed to a complex emplacement history. The same plots are shown for every sample that was dated in this study in Figure S3 (text footnote 1).

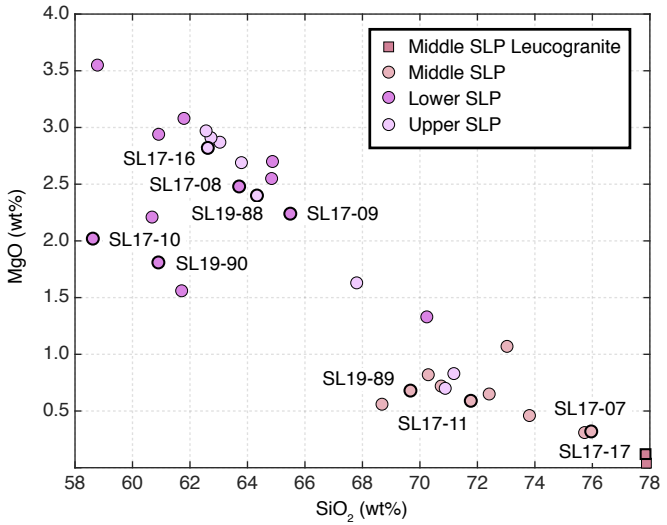

Figure 8. Comparison between the whole-rock SiO_2 (wt%) and MgO (wt%) from the Bachl et al. (2001) data set and the samples analyzed in this study from the Searchlight pluton (SLP). Our samples span most of the compositional range that was identified in previous studies.

Rare-earth element (REE) diagrams from the Lower and Upper SLP show slight Eu anomalies (0.6 < Eu/Eu* < 1) and a general enrichment in light REE over heavy REE (Figs. 10 and 11). Rare-earth element diagrams for the Middle SLP show variable depletion in the middle REE (MREE), with samples showing low to moderate depletion in MREE relative to samples of the Lower and Upper SLP and samples of leucogranite showing marked depletion of MREE (Dy_{CN}/Yb_{CN} < 1.5). The Eu anomalies for samples of the Middle SLP range from those similar to the Lower and Upper SLP to significantly more negative (Eu/Eu* < 0.5). The magnitude of the Eu/Eu* anomaly within the Middle SLP is related to SiO_2 content with the exception of the sample with the lowest SiO_2, while the Lower and Upper SLP shows no clear relationship between SiO_2 and Eu/Eu* (Fig. 10). However, all three map units show a negative correlation between Dy/Yb and SiO_2 (Fig. 10).

The results of our chemostratigraphic study of the Searchlight pluton are shown on Figure 12. They show that concentrations of Rb, Sr, and Ba in the Lower SLP do not systematically vary relative to paleo-vertical, with the exception of a zone of elevated Ba corresponding to the presence of potassium feldspar megacrysts (Fig. 12). A major break in Ba and Sr concentrations exists between the Lower and Middle SLP (Fig. 12), whereas Rb concentrations remain constant across that boundary (Fig. 12). Within the Middle SLP, Sr, Ba, and Rb concentrations are constant through the lower part of the unit but systematically change toward lower (Ba, Sr) or higher (Rb) concentrations toward the top (Fig. 12).

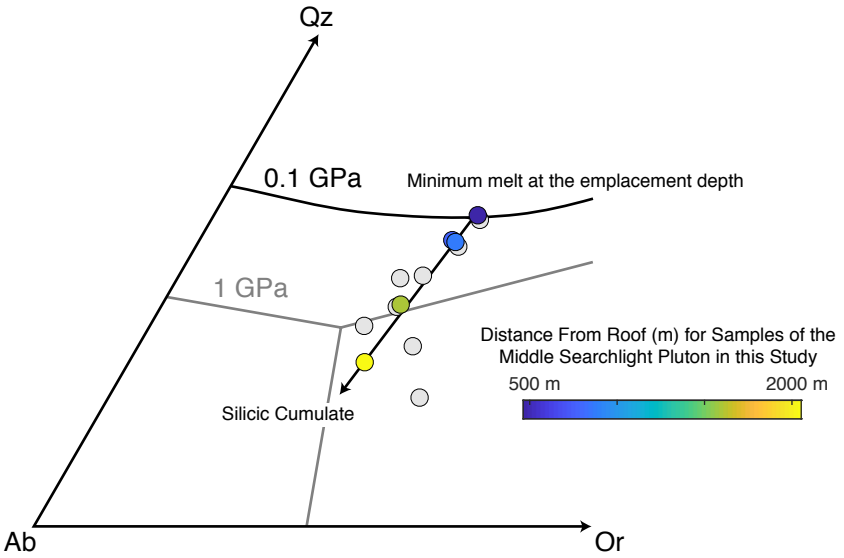

Figure 9. CIPW norms from samples of the Middle Searchlight pluton (SLP) plotted on the Qz-Ab-Or ternary. All data are projected onto the system using the correction for normative An from Blundy and Cashman (2001). The samples are color coded relative to their position beneath the roof of the pluton. Whole-rock data from the Middle SLP presented in Bachl et al. (2001) are shown as gray circles for comparison. The data from this study define a linear array that terminates at the 0.1 GPa minimum for the haplogranitic system. We interpret this array to represent a mixing line between a feldspar-dominated silicic cumulate and residual, minimum melt. The ratio of silicic cumulate relative to residual melt increases with depth, which we interpret to represent in situ differentiation of a silicic parent melt due to gravitational processes.

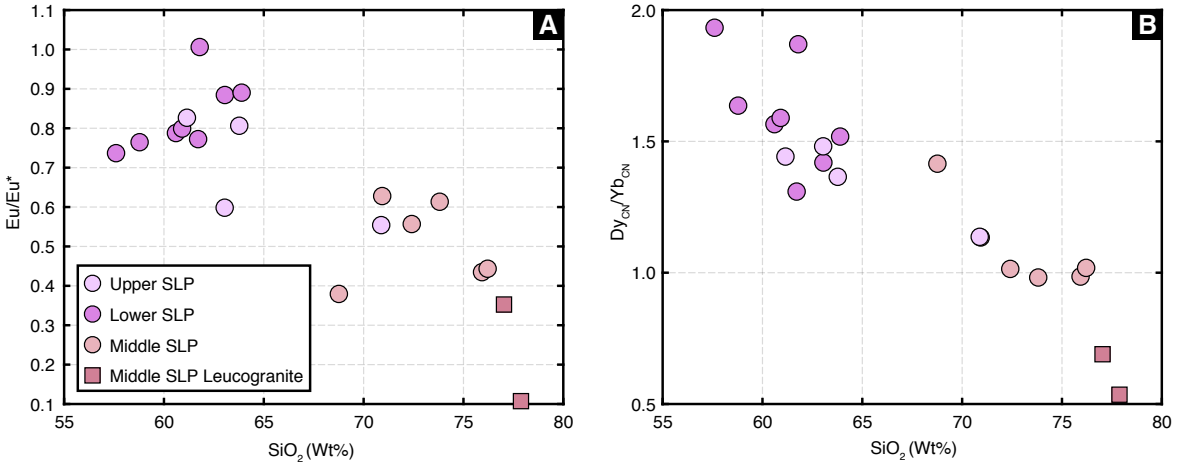

Figure 10. Comparison of SiO_2 (wt%) and Eu/Eu* (A) and Dy_{CN}/Yb_{CN} (B) for whole-rock compositions reported in Bachl et al. (2001) and this study.

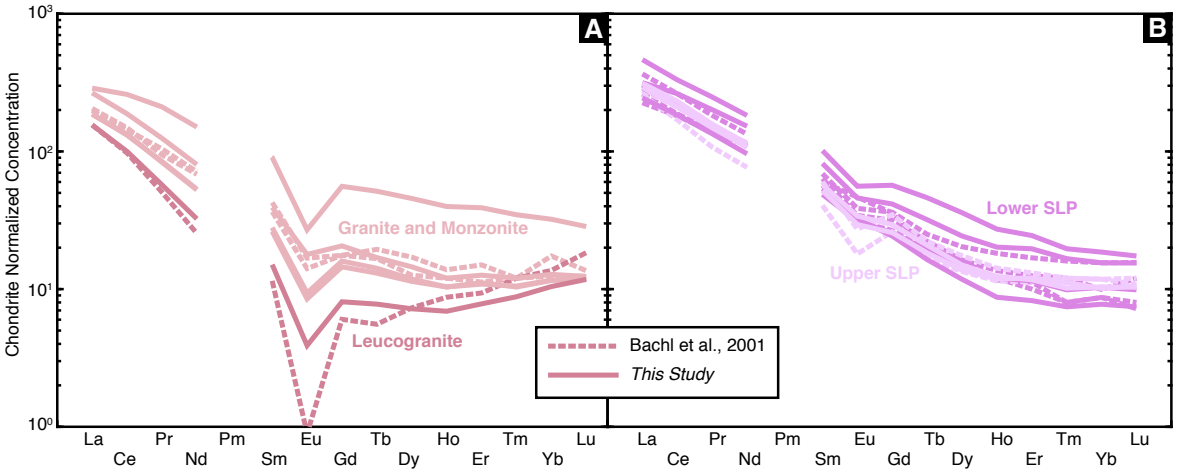

Figure 11. Chondrite-normalized, rare-earth element (REE) plots for whole-rock compositions reported in Bachl et al. (2001; dashed lines) and this study (solid lines) for the Middle (A) and Lower and Upper Searchlight pluton (SLP) (B). Note that the samples of the high-SiO_2 leucogranite show marked depletion in middle REE that is best explained by extraction of this melt from source that was crystallizing titanite (e.g., Bachmann and Bergantz, 2008; Glazner et al., 2008; Colombini et al., 2011).

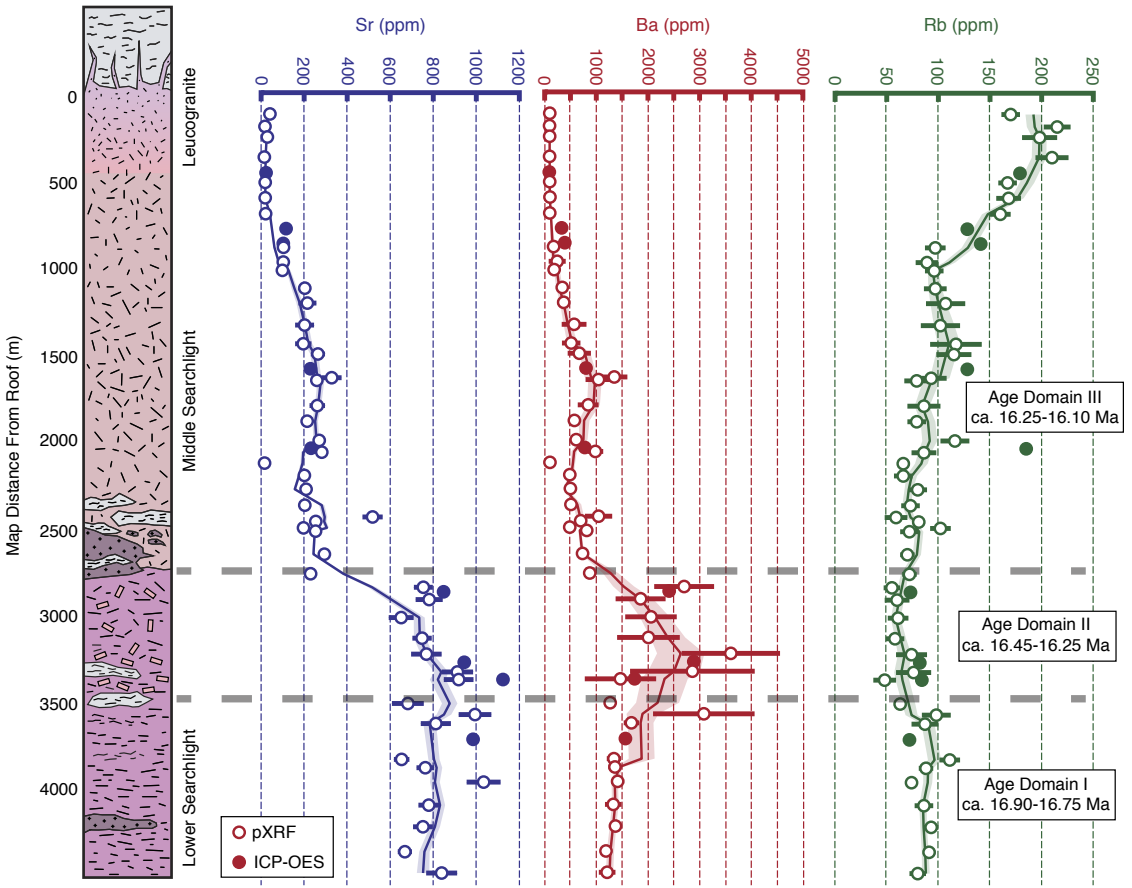

Figure 12. The magmatic stratigraphy of the Lower and Middle Searchlight pluton (SLP) along our sampling transect (please note that the Upper SLP is not present in our study area) based on portable X-ray fluorescence (pXRF) and inductively coupled plasma mass spectrometry (ICP-MS) data for Sr, Ba, and Rb. A major geochemical break between the Lower and Middle SLP suggests that there was little interaction between these two units despite a gradational contact over ~10–20 m in the field. Within the Lower SLP, there is limited geochemical variation. However, there is significant variation in the Middle SLP whereby compatible Sr and Ba are enriched near the bottom, and incompatible Rb is enriched near the top. This stratification is parallel to paleo-vertical and is consistent with gravitationally driven differentiation in this unit. To aid in visualization of the geochemical trends, a four-point running mean is shown as a solid line. The 95% confidence interval (shaded region) of the running mean was estimated by randomly resampling from the analytical uncertainty of each point, recalculating a four-point running mean for each draw, and finding the 2.5% and 97.5% lower and upper bounds of the running means. ICP-OES—inductively coupled plasma–optical emission spectroscopy.

5. DISCUSSION

5.1 Construction of the Searchlight Pluton

Our U-Pb zircon geochronology indicates that the studied parts of the Searchlight pluton were constructed over ~1.5 m.y., with the Lower and Upper SLP constructed between 17.50 and 16.25 Ma and the Middle SLP constructed between 16.25 and 16.10 Ma (Fig. 5A). Since most samples from the Lower and Upper SLP show only minor inter-sample overlap in zircon dates, we interpret these parts of the pluton to have been emplaced incrementally. The size and geometry of these increments remain unknown because our sampling density is not high enough to delineate these features within the Lower and Upper SLP. However, geochemical and textural observations indicate at least two age domains within our sampling transect.

In our study area, the oldest sample is SL17-09. It was collected from a thin (<10-m-thick) screen between large xenoliths (>>10 m in thickness and length) that form a semi-continuous zone across the pluton (Fig. 1). So, while this sample represents an early intrusion within the Searchlight magmatic system, it does not appear to be volumetrically significant within our sampling transect. Below the xenolith zone, a single sample (SL17-08) was found to contain zircon crystals dated between 16.90 and 16.75 Ma (Fig. 5A). The whole-rock trace-element geochemistry of this zone is variable (Fig. 12) and is texturally distinct from the potassium feldspar megacryst-bearing Lower SLP above the xenolith zone. Thus, this area likely represents emplacement of one or more

increments of magma. Above the xenolith zone, we have zircon dates from two samples (SL17-10 and SL19-90) that show some overlap in the age range 16.45–16.25 Ma (Fig. 5A). This part of the Lower SLP also contains abundant potassium feldspar megacrysts (cm-scale) and is texturally and geochemically distinct (see Ba in Fig. 12) from the underlying and overlying parts of the intrusive complex. This zone may also represent one or more increments of magma emplaced into the Lower SLP.

The four dated samples from the Middle SLP contain zircon grains that represent a narrow range of dates between 16.25 and 16.10 Ma (Fig. 5A), with substantial inter-sample overlap. These overlapping zircon dates indicate that this unit contained melt contemporaneously within our sampling transect. This unit is also geochemically and texturally distinct from the adjacent Lower SLP, as there is a break in whole-rock trace-element concentrations at the boundary between the Middle and Lower SLP, and the Middle SLP lacks megacrystic potassium feldspar (Fig. 12). The preservation of this geochemical discontinuity is interesting, because the youngest zircon from the Lower SLP overlaps in age with the oldest zircon from the Middle SLP (Fig. 5A), and the boundary between these two units appears gradational over 10–20 m. These observations suggest that parts of the uppermost Lower SLP were not completely solid prior to the emplacement of the Middle SLP. Nevertheless, the break in whole-rock geochemistry at the contact between these two map units (Fig. 12) indicates that any zone of mixing and homogenization was limited to the very top of the Lower SLP.

Importantly, our new geochronologic data challenge previous interpretations and studies that treated the entire Searchlight pluton as a coherent, fossil magma reservoir containing a roof solidification front (Upper SLP), extracted residual melt (Middle SLP), and silicic cumulates (Lower SLP) (Bachl et al., 2001; Gelman et al., 2014). Rather, our geochronologic data show that the Lower and Upper SLP were constructed incrementally over ~1.25 m.y. and that some increments of magma had completely crystallized prior to the emplacement of others. The preservation of a geochemical break between the uppermost Lower SLP and the Middle SLP in our sampling transect further suggests that the Lower SLP had largely crystallized prior to emplacement of the Middle SLP. These interpretations are consistent with those made following the publication of Bachl et al. (2001) from field, geochemical, and geochronologic data (Miller et al., 2006; C. Miller and G. Gualda, 2017, personal commun.). While these data preclude the originally proposed genetic relationship between the Lower, Middle, and Upper Searchlight pluton (Bachl et al., 2001; Gelman et al., 2014), our data show contemporaneous zircon crystallization over a wide area of the Middle SLP, indicating this portion of the pluton likely represents a fossil magma reservoir.

5.2 Melt Residence within the Searchlight Pluton

Most of our dated samples exhibit some degree of age dispersion beyond that expected from analytical considerations alone. We exclude the possibility that this dispersion is an analytical artifact based on the excellent reproducibility of synthetic and natural U-Pb reference materials in the Princeton geochronology laboratory (Eddy et al., 2019; Schoene et al., 2019). Potential sources of geological scatter might include incorporation of xenocrysts or antecrysts (Miller et al., 2007) or in situ zircon crystallization over timescales greater than our analytical resolution. In our analyses of zircon from the Searchlight pluton, we did not encounter any obvious inherited zircon cores in the form of distinct CL textures (Fig. S1 [footnote 1]) or any discordant U-Pb dates. Consequently, we posit that the magmas that built the pluton were intruded above their zircon saturation temperatures (e.g., Miller et al., 2003) and contain limited antecrysts and xenocrysts. Indeed, the only obvious antecrysts are two zircons from the Middle SLP leucogranite that are substantially older than the rest of the grains from that sample (Fig. 5A). For the rest of the samples, we interpret the age dispersion to record part of the interval between zircon saturation and the solidus. This duration is ~150 k.y. for most of the samples but ~300 k.y. for one sample of the Upper SLP and ~50 k.y. for the Middle SLP leucogranite (Fig. 5B). These durations should be considered minimum estimates for the duration of magma emplacement and crystallization, because (1) it is impossible for zircon to record the interval of time that the magma spent at temperatures above zircon saturation; (2) there is difficulty in sampling small domains that grew at low melt fractions; and (3) there is a tendency for low-n geochronologic data sets to underestimate duration when the analytical precision is small relative to the duration of interest (e.g., Glazner and Sadler, 2016).

Figure 6 demonstrates that our zircon trace-element data set contains compositional trends that are consistent with magmatic differentiation. We can leverage the relationships between these data to assess how well the ID-TIMS dates record the temperature interval over which zircon crystallized. For example, the Hf content of zircon grains analyzed via TIMS-TEA corresponds to the majority of the high- and medium-temperature portions of the Ti versus Hf curve (Fig. 6), suggesting that our TIMS-TEA data set is only missing the lowest temperature portion of the zircon crystallization sequence. Temperatures calculated from Ti-in-zircon thermometry (Ferry and Watson, 2007), using reasonable values of $aSiO_2 = 1$ and $aTiO_2 = 0.7$ for a late-stage silicic melt that is saturated with quartz and titanite (Hayden and Watson, 2007; Colombini et al., 2011), suggest that the TIMS-TEA data set is missing the temperature interval between the solidus and ~718 ± 32 °C. Experimental data suggest that the haplogranitic solidus at 0.2 GPa is between 680 °C and 712 °C for $aH_2O = 1.0$ and 0.70, respectively (Ebadi and Johannes, 1991), indicating that the missing temperature interval is likely small. Although, the amount of time spent near the solidus is difficult to estimate due to significant crystallization of silicic melts at this temperature and the buffering effect that the associated release of latent heat has on a magma reservoir's temperature (e.g., Huber et al., 2009).

It is also difficult to constrain the interval of time that the magmas within the Searchlight pluton spent at temperatures above zircon saturation, because zircon saturation temperatures can be spurious when calculated from granitoid compositions that do not represent liquid compositions (Barnes et al., 2019).

Colombini (2009) noted the presence of zircon in trachyandesitic, trachydacitic, low-SiO_2 rhyolites, and high-SiO_2 rhyolites in the overlying, and broadly coeval, Highland Range volcanics, suggesting that zircon saturated fairly early within the Searchlight magmatic system. These observations are further supported by Ti-in-zircon temperatures from the volcanics that range from 900 °C to 700 °C (Colombini et al., 2011). Similar Ti-in-zircon temperatures can be calculated from the data set presented in Figure 6 and Table S2 (footnote 1) using the same activities as Colombini et al. (2011): $aSiO_2 = 1$ and $aTiO_2 = 0.7$. However, while the near-solidus temperatures from these data sets are likely reliable, the higher temperatures should be considered maximums because zircon likely saturated prior to quartz and titanite within the Searchlight magmatic system. Nevertheless, we consider it unlikely that initial cooling above zircon saturation would result in long periods of unrecorded time for two reasons. First, magmas with low crystallinity will more easily convect and cool faster (Huber et al., 2009). Secondly, the preservation of a break-in whole-rock geochemistry at the boundary between Lower and Middle SLP suggests that, despite some overlap in zircon $^{206}Pb/^{238}U$ dates in samples across this boundary, the two units did not efficiently mix and homogenize. This observation places a limit on how long the magmas that formed the Middle SLP could have been assembling at temperatures above zircon saturation and indicates that this missing time interval is not resolvable within our analytical precision of ~<100 k.y.

We conclude that our zircon TIMS-TEA data sets for each sample record most of the temperature interval over which zircon crystallized. We estimate that we are missing up to 100 k.y. of magma residence prior to zircon saturation and an unconstrained amount of time at temperatures near the solidus. Our data support the conclusions of previous studies that have shown that whole-grain CA-ID-TIMS U-Pb zircon data sets will capture the same duration as carefully selected grain fragments (Samperton et al., 2015) and that meaningful age-temperature-compositional curves can be derived from such data sets (Samperton et al., 2017). Overall, our data suggest that increments of magma within the Searchlight pluton contained melt for periods of at least 50–300 k.y. Thermal modeling estimates upper-crustal residence times of silicic magmas to 10^4–10^6 yr depending on the emplacement rate, the thermal maturation of the system (e.g., Annen, 2009; Gelman et al., 2013), and the local geotherm (Karakas et al., 2017). Hydrothermal circulation above magma reservoirs will cause much faster cooling (e.g., Glazner, 2020) but is frequently ignored in thermal models. Extensive evidence for hydrothermal activity above the Searchlight pluton exists in the form of mineralized veins and highly altered host rock (Callaghan, 1939), suggesting that this process likely played an important role in modulating melt residence within this system.

Interestingly, only a few samples show temporal trends in zircon compositions that are compatible with monotonic cooling (e.g., SL19-89; Fig. 7). Instead, many show no clear geochemical trends with time (e.g., SL17-07; Fig. 8) or trends opposite to those expected for a monotonically cooling magma reservoir (e.g., SL17-09; Fig. 7). We propose two possible explanations for the absence of the predicted geochemical trends with respect to time in many of our samples. (1) Our dates are simply not precise enough to identify the trends in some samples. For example, in many of our samples, the age dispersion is equal to (SL17-07; Fig. 7), or only slightly higher than (SL17-08, -10, -11, -17, SL19-88, -90; Fig. S3 [footnote 1]), the expected dispersion from analytical uncertainty, and any temporal trends in geochemical data may be obscured. (2) Complex emplacement processes led to a history of magma composition and temperature that does not reflect monotonic cooling at the hand-sample scale. Recycling of antecrystic zircon grains that integrated different time intervals of crystallization within a magma batch or convective mixing of zircon grains from parts of the magma reservoir with different thermal histories would further act to complicate any expected trends in zircon chemistry with time (Fig. 7). In this case, integrating large volumes of each crystal might produce mean dates and trace-element concentrations that obscure rapid changes in melt temperature and composition (e.g., Kent and Cooper, 2018). In the future, smaller subsampling combined with high-precision geochronology may better elucidate these complex trends. Ultimately, we prefer a combination of these two explanations for our data from the Searchlight pluton. For example, the reproducible relationships between Hf, Eu/Eu*, and Dy_{CN}/Yb_{CN} in Middle SLP zircon compositions (Fig. 6) suggest that temporal trends in zircon compositions in samples SL17-07, SL17-11, and SL17-17 are obscured by geochronologic data that are imprecise relative to the duration of magma cooling and crystallization. On the other hand, the lack of a clear relationship between Eu/Eu* and Hf in Lower and Upper SLP zircon compositions (Fig. 6), along with the absence of clear temporal trends, or unexpected temporal trends (Fig. 7), suggests that these parts of the pluton may record a complicated cooling and crystallization history.

5.3 Differentiation within the Searchlight Pluton

A variety of processes have been proposed for crystal-liquid separation in silicic magma reservoirs including crystal settling (e.g., Tuttle and Bowen, 1958; Bachmann and Bergantz, 2004; Lee and Morton, 2015), compaction (Bachmann and Bergantz, 2004), doubly diffusive boundary layers (Huppert and Sparks, 1984), solidification front instabilities (Marsh, 2002), and extraction through dikes (Eichelberger et al., 2006; Bartley et al., 2018; Glazner et al., 2020). Here we focus on those most commonly discussed in the current literature—crystal settling and compaction (Bachmann and Bergantz, 2004; Lee and Morton, 2015; Bachmann and Huber, 2019)—which can also occur in the presence of a widespread gas phase (i.e., filter-pressing; Sisson and Bacon, 1999).

Melt fraction plays an important role in determining how crystal settling and compaction operate. At high melt fractions, crystals can sink freely and efficiently (Bachmann and Bergantz, 2004). However, this process is likely disrupted by convection while the magma's melt fraction is high and its bulk viscosity is relatively low (Shaw, 1965). On the other hand, compaction can occur at low melt fractions through viscous deformation of a crystalline framework (e.g., McKenzie, 1987). The timescales required for this process are compatible with the lifespans of some plutonic complexes (e.g., Bachmann

and Bergantz, 2004). Yet, there is little microstructural evidence within upper-crustal granitoids for viscous compaction (Holness, 2018). Instead, crystal liquid separation is thought to occur over a discrete melt extraction window between the initial development of a loose crystalline framework and rheological lock-up of the magma. The precise boundaries of this melt extraction window remain uncertain. Experimental data suggest that rigid crystalline frameworks can form in basalts at crystallinities as low as 25% (Philpotts et al., 1998), while eruptions of crystal-rich dacite suggest that silicic magmas do not reach complete rheological lock-up until 40%–50% crystallinity (Hildreth, 1981).

The processes that occur within the melt extraction window are complex and may involve the formation of fragile, stress-bearing crystalline lattices that can later collapse as conditions within the magma reservoir change (Bergantz et al., 2017). Mechanical rotation of grains into more efficiently packed configurations during collapse, termed micro-settling (Bachmann and Bergantz 2004) or mechanical compaction (Holness 2018), ultimately helps reduce porosity and expel residual melt upward. Importantly, since the driving force of this process is gravity, it should result in the development of a geochemical gradient parallel to paleo-vertical that reflects the distribution of early-formed crystals and residual melt. In the following sections, we separately discuss the record of this process within the Middle SLP and Lower and Upper SLP.

5.3.1 Middle Searchlight Pluton

The narrow range of zircon dates within the Middle SLP, at least within our sampling transect, indicates that this unit contained melt simultaneously between 16.25 and 16.10 Ma and that it could represent an ~2.7-km-thick fossil magma reservoir. Our geochemical data demonstrate that this unit is stratified with respect to paleo-vertical, suggesting gravity played a major role in its differentiation (Figs. 9 and 12). Compatible elements in feldspar (Sr and Ba) show moderate concentrations (~200 ppm Sr and ~500 ppm Ba) in the bottom of the unit and a change toward extremely low concentrations (close to zero ppm) at the top. Rubidium, which is largely incompatible in silicic melts, is uniformly near 100 ppm through the bottom of the unit but gradually increases to 200 ppm toward the top. These results are consistent with accumulation of early-formed crystals near the bottom of the unit and increased residual melt near the top. The samples from the top of the unit, including its leucogranite cap, also plot near the 0.1 GPa haplogranitic minimum, while those from deeper in the Middle SLP form a linear array toward increasingly feldspar-rich compositions. The former is interpreted to represent the composition of melt extracted from a quartz- and feldspar-bearing crystalline mush at the emplacement depth (Fig. 9). The latter reflects an increasing fraction of early-formed feldspar with depth. These trends are similar to those inferred to exist in the silicic magma reservoirs that feed zoned ignimbrites (Hildreth, 1981).

We can use the geochemistry of the extracted high-SiO_2 magma (leucogranite capping the Middle SLP) to place constraints on the state of the magma reservoir during the segregation process. First, the leucogranite has a composition equivalent to the haplogranitic minimum at the emplacement depth of the Middle SLP, indicating that the parent melt was saturated in both quartz and feldspar prior to segregation. Second, whole-rock REE diagrams for Middle SLP samples show that the high-SiO_2 leucogranite is distinctly depleted in MREE relative to samples of the underlying granite and quartz monzonite (Figs. 10 and 11). This relationship implies that the high-SiO_2 melt was removed from a source that was crystallizing titanite (Bachmann and Bergantz, 2008; Glazner et al., 2008; Colombini et al., 2011). Colombini et al. (2011) did a comprehensive study of titanite in rhyolite erupted from the Searchlight magmatic system and demonstrated that it began to crystallize in these magmas after zircon saturation and at relatively low temperatures (<755 °C). It is therefore likely that segregation of the high-SiO_2 leucogranite from the rest of the Middle SLP did not occur until fairly late in its magmatic history. Third, there is no clear field evidence for the leucogranite's extraction from the underlying granite and quartz monzonite through dikes (e.g., Eichelberger et al., 2006, Bartley et al., 2018; Glazner et al., 2020), and the smooth geochemical gradients between the leucogranite and underlying units (Fig. 9 and 12) are inconsistent with an intrusive relationship between the two. In combination, these observations require the magma reservoir had the following properties when melt was segregated: (1) it had cooled and crystallized enough to have reached the granitic minimum at the emplacement level (680 °C to 712 °C at 2 kbar for $aH_2O = 1$ and 0.7, respectively: Ebadi and Johannes, 1991); (2) it was saturated in titanite (<755 °C, Colombini et al., 2011); and (3) it had not reached the threshold for rheological lockup (>25 vol% and <55 vol% crystals: Vigneresse et al., 1996; Philpotts et al., 1998).

Our constraints require moderate crystallinity at the granitic minimum and provide further support for models in which the majority of crystallization occurs near the solidus in dacitic to rhyolitic magmas (e.g., Huber et al., 2009; Gelman et al., 2013). They are also consistent with extraction and segregation of residual melt by a gravitationally driven process. The depth-dependence of compositions within the Middle SLP is particularly consistent with melt segregation via compaction. Yet, we are aware of no evidence within the Middle SLP, or most other upper-crustal granitoid plutons (Holness, 2018), for compaction via viscous deformation of a crystalline framework. Instead, we suggest that this process occurred via depth-dependent repacking of crystals (e.g., Bachmann and Huber, 2019).

As discussed above, CA-ID-TIMS-TEA U-Pb zircon geochronology will not record magma residence prior to zircon saturation and the difficulty of sampling small growth domains means that our data will also miss an unconstrained period of magma residence at near-solidus temperatures. Despite these limitations, we can use our constraints on the state of the magma reservoir during segregation of high-SiO_2 magma in concert with our zircon geochronology to determine the timescales over which differentiation and melt segregation occurred. In particular, if zircon saturated prior to titanite in all of the magmas within the Searchlight magmatic system (Colombini et al., 2011), then it is likely that our U-Pb data set for the Middle SLP includes a period of time prior to

melt extraction. Similarly, most crystallization-temperature curves for H_2O-rich silicic melts predict that rheological lockup will happen at temperatures slightly above the solidus (Huber et al., 2009; Gelman et al., 2013; Hartung et al., 2019). Since our TIMS-TEA data indicate that the analyzed zircon from the Middle SLP include some grains that record near-solidus temperatures, we think it is likely that the dates encompass this rheological boundary. These constraints suggest that the observed zircon age dispersion in the Middle SLP provides a maximum duration for high-SiO_2 melt extraction and that this process occurred in <150 k.y. within the longer >200–250 k.y. evolution of the Middle SLP magmatic reservoir.

5.3.2 Lower and Upper Searchlight Pluton

Whether crystal-liquid separation occurred within any of the intrusions that incrementally built the Lower and Upper SLP is difficult to determine. Textural and geochemical heterogeneity within the Lower and Upper SLP can be used to infer that increments were much smaller than the Middle SLP magma reservoir. These units were emplaced earlier within the magmatic system's history, when cooling rates should have been highest. Nonetheless, the inferred longevity of melt within the Lower and Upper SLP is similar to or longer than that of melt within the Middle SLP based on zircon U-Pb age dispersion (Fig. 5B). Thus, these magmas likely did not rapidly quench in the upper crust and may have had enough time to differentiate. Yet, we find no systematic variation in the concentration of Sr or Rb with respect to paleo-vertical in our sampling transect of the Lower SLP (Fig. 12). The lack of any systematic paleo-vertical geochemical trends suggests several possibilities: (1) the individual magma increments that built this unit did not differentiate due to gravitationally driven processes; (2) differentiation occurred at length scales that were too small to be captured by our sample spacing of 100–200 m; or (3) that any extracted melt was mixed into subsequent intrusive pulses or erupted. We explore these possibilities below.

If the magmas that built the Lower and Upper SLP did not undergo crystal-liquid separation within the upper crust, then their compositions might reflect melts extracted at depth and frozen at the emplacement level. If so, the bulk of the SiO_2 variability in the Searchlight magmatic system would reflect deep crustal magmatic processes, and only the Middle SLP would have differentiated in the upper crust. This is a similar interpretation to that of Coleman et al. (2012) for granitoids within the Tuolumne Intrusive Suite, where they found evidence for limited differentiation within km-scale sills (similar to the Middle SLP) but attributed most geochemical variation within the larger batholith to magmatic processes in the lower crust. It is also similar to the conclusions drawn by Lee and Morton (2015), who attributed two distinct differentiation trends in Harker diagrams of plutonic rock compositions from the Peninsular Ranges Batholith to lower-crustal processes (~45–70 wt% SiO_2) and upper-crustal differentiation of silicic melts (~70–77 wt% SiO2). However, the magmas that crystallized to form the Lower and Upper SLP were presumably more mafic than the parent magma for the Middle SLP and should have more efficiently undergone gravitationally driven differentiation due to crystallization of a larger volume of dense, mafic minerals and a lower melt viscosity. Therefore, it is difficult to reconcile the lack of systematic vertical geochemical variation in the Lower SLP (Fig. 12) with the apparent longevity of melt within each dated sample (Fig. 5B).

Another possibility is that the magmas that built the Lower and Upper SLP differentiated but any extracted melt was either erupted or mixed into subsequent pulses of magma. Mixing is certainly possible between the uppermost Lower and Middle SLP, where the age difference between the units is small (Fig. 5A). We interpreted the preservation of a geochemical break between these units (Fig. 12) to indicate that the uppermost Lower SLP was behaving rigidly when the Middle SLP was emplaced. However, this interpretation does not preclude mixing a melt-rich cap from this part of the Lower SLP into the Middle SLP. Indeed, Ba concentrations in the uppermost Lower SLP (up to ~3000 ppm: Fig. 12) are higher than trachyandesite and trachydacite lava compositions (~1500 ppm) in the overlying Highland Range volcanics and may indicate accumulated alkali feldspar relative to potential parent melts. Our geochronologic data are not dense enough to determine if adjacent increments of the Lower and Upper SLP are close in age outside of our main sampling transect. If so, progressive mixing might be a viable explanation for the lack of clear gravitationally driven differentiation trends within these units. Subtle isotopic differences between the plutonic units (Bachl et al., 2001) may offer a next step in testing this hypothesis.

Eruption of extracted, residual magma from the Lower and Upper SLP provides a final potential explanation for the apparent absence of differentiation in these units. In this case, future studies of the Highland Range volcanics can compare eruptive compositions with age-equivalent parts of the pluton to assess whether they are complementary. However, the absence of clear zones of extracted residual melt within these plutonic units would suggest that any eruptions were either very efficient or subsequently obscured through further intrusion and mixing.

6. CONCLUSIONS

High-precision U-Pb zircon geochronology shows that the Middle SLP simultaneously contained melt over a large area and that it represents a fossil magma reservoir that was extant for ~200 k.y. Geochemical gradients with respect to compatible and incompatible elements within this reservoir are parallel to paleo-vertical and suggest that it differentiated due to gravitationally driven processes. The longevity and geochemical structure of the Middle SLP is compatible with the inferred structure of the magma reservoirs that source high-SiO_2 rhyolite eruptions and offers a unique opportunity to study the processes that occur in these systems at depth. We infer that melt segregation occurred through mechanical rearrangement of crystals at moderate crystallinity, and that this process occurred over a short interval (<<150 k.y.) in

the longer history of the Middle SLP magma reservoir. The Lower and Upper SLP predate this fossil magma reservoir and were incrementally emplaced. Compositions from these units appear to represent melts that have undergone very little upper-crustal differentiation with compositions reflective of magmatic processes in the deep crust or that represent the products of in situ differentiation over a much smaller scale than the Middle SLP. If differentiation did occur in these units, any extracted residual melt was either efficiently erupted or mixed subsequent increments of magma within the pluton.

ACKNOWLEDGMENTS

We thank C. Miller, J. Miller, G. Gualda, B. Wallrich, J. Faulds, and N. Hinz for discussions about the Searchlight magmatic system and for guidance in the field. We are particularly grateful for C. Miller's willingness to share his decades of experience in the area. This paper benefited from thoughtful reviews by C. Miller and L. Caricchi, as well as the editorial handing of G. Gualda and S. de Silva. This project was supported by National Science Foundation (NSF) grants EAR-1830937 to B. Schoene and EAR-2007057 to A. Pamukçu. The ion microprobe laboratory at UCLA is partially funded by a grant from NSF Earth Science Instrumentation and Facilities Program (1734856).

REFERENCES CITED

Annen, C., 2009, From plutons to magma chambers: thermal constraints on the accumulation of eruptible silicic magma in the upper crust: Earth and Planetary Science Letters, v. 284, p. 409–416, https://doi.org/10.1016/j.epsl.2009.05.006.

Annen, C., Blundy, J.D., Leuthold, J., and Sparks, R.S.J., 2015, Construction and evolution of igneous bodies: Towards an integrated perspective of crustal magmatism: Lithos, v. 230, p. 206–221, https://doi.org/10.1016/j.lithos.2015.05.008.

Bachl, C.A., Miller, C.F., Miller, J.S., and Faulds, J.E., 2001, Construction of a pluton: Evidence from an exposed cross section of the Searchlight pluton, Eldorado Mountains, Nevada: Geological Society of America Bulletin, v. 113, p. 1213–1228, https://doi.org/10.1130/0016-7606(2001)113<1213:COAPEF>2.0.CO;2.

Bachmann, O., and Bergantz, G.W., 2004, On the origin of crystal-poor rhyolites: Extracted from batholithic crystal mushes: Journal of Petrology, v. 45, p. 1565–1582, https://doi.org/10.1093/petrology/egh019.

Bachmann, O., and Bergantz, G.W., 2008, Rhyolites and their source mushes across tectonics settings: Journal of Petrology, v. 49, p. 2277–2285, https://doi.org/10.1093/petrology/egn068.

Bachmann, O., and Huber, C., 2016, Silicic magma reservoirs in the Earth's crust: American Mineralogist, v. 101, p. 2377–2404, https://doi.org/10.2138/am-2016-5675.

Bachmann, O., and Huber, C., 2019, The inner workings of crustal distillation columns: The physical mechanisms and rates controlling phase separation in silicic magma reservoirs: Journal of Petrology, v. 60, p. 3–18, https://doi.org/10.1093/petrology/egy103.

Barnes, C.G., Werts, K., Memeti, V., and Ardill, K., 2019, Most granitoid rocks are cumulates: deductions from hornblende compositions and zircon saturation: Journal of Petrology, v. 60, p. 2227–2240, https://doi.org/10.1093/petrology/egaa008.

Bartley, J.M., Glazner, A.F., and Coleman, D.S., 2018, Dike intrusion and deformation during growth of the Half Dome pluton, Yosemite National Park, California: Geosphere, v. 14, no. 3, p. 1283–1297, https://doi.org/10.1130/GES01458.1.

Bateman, P.C., and Chappell, B.W., 1979, Crystallization, fractionation, and solidification of the Tuolumne intrusive series, Yosemite National Park, California: Geological Society of America Bulletin, v. 90, p. 465–482, https://doi.org/10.1130/0016-7606(1979)90<465:CFASOT>2.0.CO;2.

Bell, E.A., Boehnke, P., and Harrison, T.M., 2016, Recovering the primary geochemistry of Jack Hills zircons through quantitative estimates of chemical alteration: Geochimica et Cosmochimica Acta, v. 191, p. 187–202, https://doi.org/10.1016/j.gca.2016.07.016.

Bergantz, G.W., Schleicher, J.M., and Burgisser, A., 2017, On the kinematics and dynamics of crystal-rich systems: Journal of Geophysical Research. Solid Earth, v. 122, p. 6131–6159, https://doi.org/10.1002/2017JB014218.

Blundy, J., and Cashman, K., 2001, Ascent driven crystallization of dacite magmas at Mount St Helens, 1980–1986: Contributions to Mineralogy and Petrology, v. 140, p. 631–650, https://doi.org/10.1007/s004100000219.

Callaghan, E., 1939, Geology of the Searchlight district Clark County, Nevada: U.S. Geological Survey Bulletin 906-D, p. 135–188, https://doi.org/10.3133/b906D.

Cates, N.L., Miller, J.S., Miller, C.F., Wooden, J.L., Erickson, S., and Means, M., 2003, Longevity of plutonic systems: SHRIMP evidence from Aztec Wash and Searchlight plutons, Nevada: Geological Society of America Abstracts with Programs, v. 35, p. 63.

Claiborne, L.L., Miller, C.F., Walker, B.A., Wooden, J.L., Mazdab, F.K., and Bea, F., 2006, Tracking magmatic processes through Zr/Hf ratios in rocks and Hf and Ti zoning in zircons: An example from the Spirit Mountain batholith, Nevada: Mineralogical Magazine, v. 70, p. 517–543, https://doi.org/10.1180/0026461067050348.

Claiborne, L.L., Miller, C.F., Gualda, G.A.R., Carley, T., Covey, A.K., Wooden, J.L., and Fleming, M.A., 2018, Zircon as magma monitor, *in* Moser, D.E., Corfu, F., Darling, J.R., Reddy, S.M., and Tait, K., eds., Microstructural Geochronology: Planetary Records Down to Atom Scale: American Geophysical Union, Geophysical Monograph Series, v. 232, p. 1–33, https://doi.org/10.1002/9781119227250.ch1.

Coleman, D.S., Gray, W., and Glazner, A.F., 2004, Rethinking the emplacement and evolution of zoned plutons: Geochronologic evidence for incremental assembly of the Tuolumne intrusive suite, California: Geology, v. 32, p. 433–436, https://doi.org/10.1130/G20220.1.

Coleman, D.S., Bartley, J.M., Glazner, A.F., and Pardue, M.J., 2012, Is chemical zonation in plutonic rocks driven by changes in source magma composition or shallow-crustal differentiation?: Geosphere, v. 8, p. 1568–1587, https://doi.org/10.1130/GES00798.1.

Colombini, L.L., 2009, Mid-Miocene rhyolite sequence, Highland Range, NV: Record of magma evolution and eruption from the Searchlight pluton magma chamber [M.S. thesis]: Nashville, Tennessee, Vanderbilt University, 318 p.

Colombini, L.L., Miller, C.F., Gualda, G.A.R., Wooden, J.L., and Miller, J.S., 2011, Sphene and zircon in the Highland Range volcanic sequence (Miocene, southern Nevada, USA): Elemental partitioning, phase relations, and influence on evolution of silicic magma: Contributions to Mineralogy and Petrology, v. 102, p. 29–50, https://doi.org/10.1007/s00710-011-0177-3.

Condon, D.J., Schoene, B., McLean, N.M., Bowring, S.A., and Parrish, R.R., 2015, Metrology and traceability of U-Pb isotope dilution geochronology (EARTHTIME Tracer Calibration Part I): Geochimica et Cosmochimica Acta, v. 164, p. 464–480, https://doi.org/10.1016/j.gca.2015.05.026.

Davis, J.W., Coleman, D.S., Gracely, J.T., Gaschnig, R., and Stearns, M., 2012, Magma accumulation rates and thermal histories of plutons of the Sierra Nevada batholith, CA: Contributions to Mineralogy and Petrology, v. 163, p. 449–465, https://doi.org/10.1007/s00410-011-0683-7.

Deering, C.D., Keller, B., Schoene, B., Bachmann, O., Beane, R., and Ovtcharova, M., 2016, Zircon record of the plutonic-volcanic connection and protracted rhyolite melt evolution: Geology, v. 44, p. 267–270, https://doi.org/10.1130/G37539.1.

Dufek, J., and Bachmann, O., 2010, Quantum magmatism: magmatic compositional gaps generated by melt-crystal dynamics: Geology, v. 38, p. 687–690, https://doi.org/10.1130/G30831.1.

Ebadi, A., and Johannes, W., 1991, Beginning of melting and composition of first melts in the system Qz-Ab-Or-H_2O-CO_2: Contributions to Mineralogy and Petrology, v. 106, p. 286–295, https://doi.org/10.1007/BF00324558.

Eddy, M.P., Bowring, S.A., Miller, R.B., and Tepper, J.H., 2016, Rapid assembly and crystallization of a fossil, large-volume silicic magma chamber: Geology, v. 44, p. 331–334, https://doi.org/10.1130/G37631.1.

Eddy, M.P., Ibañez-Mejia, M., Burgess, S.D., Coble, M.A., Cordani, U.G., DesOrmeau, J., Gehrels, G.E., Li, X., MacLennan, S., Pecha, M., Sato, K., Schoene, B., Valencia, V.A., Vervoort, J.D., and Wang, T., 2019, GHR1 Zircon—A new Eocene natural reference material for microbeam U-Pb geochronology and Hf isotopic analysis of zircon: Geostandards and Geoanalytical Research, v. 43, p. 113–132, https://doi.org/10.1111/ggr.12246.

Eichelberger, J.C., Izbekov, P.E., and Browne, B.L., 2006, Bulk chemical trends at arc volcanoes are not liquid lines of descent: Lithos, v. 87, p. 135–154, https://doi.org/10.1016/j.lithos.2005.05.006.

Faulds, J.E., Feuerbach, D.L., Miller, C.F., and Smith, E.I., 2001, Cenozoic evolution of the northern Colorado River extensional corridor, southern Nevada and northwest Arizona: Pacific Section of the American Association of Petroleum Geologists Publication GB, v. 78, p. 239–272.

Faulds, J.E., Bell, J.W., and Olson, E.L., 2002a, Geologic map of the Nelson SW quadrangle Clark county, Nevada: Nevada Bureau of Mines Map 134, scale 1:24,000, 1 sheet, 15 p. text.

Faulds, J.E., Olson, E.L., Harlan, S.S., and McIntosh, W.C., 2002b, Miocene extension and fault-related folding in the Highland Range, southern Nevada: A three-dimensional perspective: Journal of Structural Geology, v. 24, p. 861–886, https://doi.org/10.1016/S0191-8141(01)00116-X.

Faulds, J.E., Ramelli, A.R., and Lledo, H., 2006, Preliminary geologic map of the north half of the Searchlight quadrangle, Clark County, Nevada: Nevada Bureau of Mines Open-File Report 2006-15, scale 1:24,000, 1 plate, 11 p. text.

Ferry, J.M., and Watson, E.B., 2007, New thermodynamic models and revised calibrations for the Ti-in-zircon and Zr-in-rutile thermometers: Contributions to Mineralogy and Petrology, v. 154, p. 429–437, https://doi.org/10.1007/s00410-007-0201-0.

Floess, D., Caricchi, L., Simpson, G., and Wallis, S.R., 2019, Melt segregation and the architecture of magmatic reservoirs: Insights from the Muroto sill (Japan): Contributions to Mineralogy and Petrology, v. 174, 15 p., https://doi.org/10.1007/s00410-019-1563-9.

Frazer, R.E., Coleman, D.S., and Mills, R.D., 2014, Zircon U-Pb geochronology of the Mount Givens Granodiorite: Implications for the genesis of large volumes of eruptible magma: Journal of Geophysical Research. Solid Earth, v. 119, p. 2907–2924, https://doi.org/10.1002/2013JB010716.

Gelman, S.E., Gutiérrez, F.J., and Bachmann, O., 2013, On the longevity of large upper crustal silicic magma reservoirs: Geology, v. 41, p. 759–762, https://doi.org/10.1130/G34241.1.

Gelman, S.E., Deering, C.D., Bachmann, O., Huber, C., and Gutiérrez, F.J., 2014, Identifying the crystal graveyards remaining after large silicic eruptions: Earth and Planetary Science Letters, v. 403, p. 299–306, https://doi.org/10.1016/j.epsl.2014.07.005.

Glazner, A.F., 2020, Climate and the Development of Magma Chambers: Geosciences, v. 10, p. 93, https://doi.org/10.3390/geosciences10030093.

Glazner, A.F., and Sadler, P.M., 2016, Estimating the duration of geologic intervals from a small number of age determinations: A challenge common to petrology and paleobiology: Geochemistry, Geophysics, Geosystems, v. 17, p. 4892–4898, https://doi.org/10.1002/2016GC006542.

Glazner, A.F., Coleman, D.S., and Bartley, J.M., 2008, The tenuous connection between high-silica rhyolites and granodiorite plutons: Geology, v. 36, p. 183–186, https://doi.org/10.1130/G24496A.1.

Glazner, A.F., Coleman, D.S., and Mills, R.D., 2018, The volcanic-plutonic connection, *in* Breitkreuz, C., and Rocchi, S., eds., Physical Geology of Shallow Magmatic Systems: Advances in Volcanology: New York, Springer International Publishing, p. 61–82, https://doi.org/10.1007/11157_2015_11.

Glazner, A.F., Bartley, J.M., Coleman, D.S., and Lindgren, K., 2020, Aplite diking and infiltration: A differentiation mechanism restricted to plutonic rocks: Contributions to Mineralogy and Petrology, v. 175, p. 37, https://doi.org/10.1007/s00410-020-01677-1.

Gualda, G.A.R., and Ghiorso, M.S., 2013, Low-pressure origin of high-silica rhyolites and granites: The Journal of Geology, v. 121, p. 537–545, https://doi.org/10.1086/671395.

Harrison, T.M., Watson, E.B., and Aikman, A.B., 2007, Temperature spectra of zircon crystallization in plutonic rocks: Geology, v. 35, no. 7, p. 635–638, https://doi.org/10.1130/G23505A.1.

Hartung, E., Caricchi, L., Floess, D., Wallis, S., Harayama, S., Kouzmanov, K., and Chiaradia, M., 2017, Evidence for residual melt extraction in the Takidani pluton, central Japan: Journal of Petrology, v. 58, p. 763–788, https://doi.org/10.1093/petrology/egx033.

Hartung, E., Weber, G., and Caricchi, L., 2019, The role of H_2O on the extraction of melt from crystallizing magmas: Earth and Planetary Science Letters, v. 508, p. 85–96, https://doi.org/10.1016/j.epsl.2018.12.010.

Hayden, L.A., and Watson, E.B., 2007, Rutile saturation in hydrous siliceous melts and its bearing on Ti-thermometry of quartz and zircon: Earth and Planetary Science Letters, v. 258, p. 561–568, https://doi.org/10.1016/j.epsl.2007.04.020.

Hiess, J., Condon, D.J., McLean, N., and Noble, S.R., 2012, $^{238}U/^{235}U$ systematics in terrestrial uranium-bearing minerals: Science, v. 335, p. 1610–1614, https://doi.org/10.1126/science.1215507.

Hildreth, W., 1981, Gradients in silicic magma chambers: Implications for lithospheric magmatism: Journal of Geophysical Research, v. 86, p. 10,153–10,192, https://doi.org/10.1029/JB086iB11p10153.

Hinz, N.H., Green, H.L., and Faulds, J.E., 2009, Preliminary geologic map of the west half of the Ireteba Peaks quadrangle, Clark County, Nevada: Nevada Bureau of Mines Open-File Report 2009-04, scale 1:24,000, 1 plate.

Hinz, N.H., Faulds, J.E., and Ramelli, A.R., 2012, Preliminary geologic map of the north half of the Fourth of July Mountain quadrangle, Clark County, Nevada: Nevada Bureau of Mines Open-File Report 2012-08, scale 1:24,000, 1 plate.

Holness, M.B., 2018, Melt segregation from silicic crystal mushes: A critical appraisal of possible mechanisms and their microstructural record: Contributions to Mineralogy and Petrology, v. 173, https://doi.org/10.1007/s00410-018-1465-2.

Hoskin, P.W.O., and Schaltegger, U., 2003, The composition of zircon and igneous and metamorphic petrogenesis, *in* Hoskin, P.W.O., and Hanchar, J.M., eds., Zircon: Reviews in Mineralogy and Geochemistry, v. 53, p. 27–62, https://doi.org/10.1515/9781501509322-005.

Huber, C., Bachmann, O., and Manga, M., 2009, Homogenization processes in silicic magma chambers by stirring and mushification (latent heat buffering): Earth and Planetary Science Letters, v. 283, p. 38–47, https://doi.org/10.1016/j.epsl.2009.03.029.

Huppert, H.E., and Sparks, R.S.J., 1984, Double-diffusive convection due to crystallization in magmas: Annual Review of Earth and Planetary Sciences, v. 12, p. 11–37, https://doi.org/10.1146/annurev.ea.12.050184.000303.

Kamiyama, H., Nakajima, T., and Kamioka, H., 2007, Magmatic stratigraphy of the tilted Tottabetsu plutonic complex, Hokkaido, North Japan: Magma chamber dynamics and pluton construction: The Journal of Geology, v. 115, p. 295–314, https://doi.org/10.1086/512754.

Karakas, O., Degruyter, W., Bachmann, O., and Dufek, J., 2017, Lifetime and size of shallow magma bodies controlled by crustal-scale magmatism: Nature Geoscience, v. 10, p. 446–450, https://doi.org/10.1038/ngeo2959.

Keller, C.B., Schoene, B., Barboni, M., Samperton, K.M., and Husson, J.M., 2015, Volcanic-plutonic parity and the differentiation of the continental crust: Nature, v. 523, p. 301–307, https://doi.org/10.1038/nature14584.

Kent, A.J.R., and Cooper, K.M., 2018, How well do zircons record the thermal evolution of magmatic systems?: Geology, v. 46, no. 2, p. 111–114, https://doi.org/10.1130/G39690.1.

Krogh, T.E., 1973, A low-contamination method for hydrothermal decomposition of zircon and extraction of U and Pb for isotopic age determinations: Geochimica et Cosmochimica Acta, v. 37, p. 485–494, https://doi.org/10.1016/0016-7037(73)90213-5.

Lee, C.T.A., and Morton, D.M., 2015, High silica granites: Terminal porosity and crystal settling in shallow magma chambers: Earth and Planetary Science Letters, v. 409, p. 23–31, https://doi.org/10.1016/j.epsl.2014.10.040.

Lipman, P.W., and Bachmann, O., 2015, Ignimbrites to batholiths: Integrating perspectives from geological, geophysical, and geochronological data: Geosphere, v. 11, no. 3, p. 705–743, https://doi.org/10.1130/GES01091.1.

Lundstrom, C.C., and Glazner, A.F., 2016, Silicic magmatism and the volcanic-plutonic connection: Elements, v. 12, p. 91–96, https://doi.org/10.2113/gselements.12.2.91.

Marsh, B.D., 2002, On bimodal differentiation by solidification front instability in basaltic magmas, part 1: Basic mechanics: Geochimica et Cosmochimica Acta, v. 66, p. 2211–2229, https://doi.org/10.1016/S0016-7037(02)00905-5.

Mattinson, J.M., 2005, Zircon U-Pb chemical abrasion ("CA-TIMS") method: Combined annealing and multi-step partial dissolution analysis for improved precision and accuracy of zircon ages: Chemical Geology, v. 220, p. 47–66, https://doi.org/10.1016/j.chemgeo.2005.03.011.

Matzel, J.E.P., Bowring, S.A., and Miller, R.B., 2006, Time scales of pluton construction at differing crustal levels: examples from the Mount Stuart and Tenpeak intrusions, North Cascades, Washington: Geological Society of America Bulletin, v. 118, p. 1412–1430, https://doi.org/10.1130/B25923.1.

McKenzie, D., 1987, The compaction of igneous and sedimentary rocks: Journal of the Geological Society of London, v. 144, p. 299–307, https://doi.org/10.1144/gsjgs.144.2.0299.

McLean, N.M., Condon, D.J., Schoene, B., and Bowring, S.A., 2015, Evaluating uncertainties in the calibration of isotopic reference materials and multi-element isotopic tracers (EARTHTIME Tracer Calibration Part II): Geochimica et Cosmochimica Acta, v. 164, p. 481–501, https://doi.org/10.1016/j.gca.2015.02.040.

Memeti, V., Paterson, S., Matzel, J.E.P., Mundil, R., and Okaya, D., 2010, Magmatic lobes as "snapshots" of magma chamber growth and evolution in large, composite batholiths: An example from the Tuolumne intrusion, Sierra Nevada, California: Geological Society of America Bulletin, v. 122, p. 1912–1931, https://doi.org/10.1130/B30004.1.

Michel, J., Baumgartner, L., Putlitz, B., Schaltegger, U., and Ovtcharova, M., 2008, Incremental growth of the Patagonian Torres del Paine laccolith over 90 k.y: Geology, v. 36, p. 459–462, https://doi.org/10.1130/G24546A.1.

Miller, C.F., McDowell, S.M., and Mapes, R.W., 2003, Hot and cold granites?: Implications of zircon saturation temperatures and preservation of inheritance: Geology, v. 31, p. 529–532, https://doi.org/10.1130/0091-7613(2003)031<0529:HACGIO>2.0.CO;2.

Miller, C.F., Furbish, D.J., Walker, B.A., Claiborne, L.L., Koteas, G.C., Bleick, H.A., and Miller, J.S., 2011, Growth of plutons by incremental emplacement of sheets in crystal-rich host: Evidence from Miocene intrusions of the Colorado River Extensional region, Nevada, USA: Tectonophysics, v. 500, p. 65–77, https://doi.org/10.1016/j.tecto.2009.07.011.

Miller, J., Miller, C., Wooden, J., Perrault, D., Hodge, K., Faulds, J., Cates, N., and Means, M., 2006, A 2 million year history of plutonism and volcanism in the Searchlight magma system, Eldorado Mountains, Nevada (USA): San Francisco, California, American Geophysical Union, Abstract V51E–1714 presented at 2006 Fall Meeting, 10–15 Dec.

Miller, J.S., Matzel, J.E.P., Miller, C.F., Burgess, S.D., and Miller, R.B., 2007, Zircon growth and recycling during the assembly of large, composite arc plutons: Journal of Volcanology and Geothermal Research, v. 167, p. 282–299, https://doi.org/10.1016/j.jvolgeores.2007.04.019.

Mills, R.D., and Coleman, D.S., 2013, Temporal and chemical connections between plutons and ignimbrites from the Mount Princeton magmatic center: Contributions to Mineralogy and Petrology, v. 165, p. 961–980, https://doi.org/10.1007/s00410-012-0843-4.

Philpotts, A.R., Shi, J., and Brustman, C., 1998, Role of plagioclase crystal chains in the differentiation of partly crystallized basaltic magma: Nature, v. 395, p. 343–346, https://doi.org/10.1038/26404.

Putnam, R., Glazner, A.F., Coleman, D.S., Kylander-Clark, A.R.C., Pavelsky, T., and Abbot, M.I., 2015, Plutonism in three dimensions: Field and geochemical relations on the southeast face of El Capitan, Yosemite National Park, California: Geosphere, v. 11, p. 1133–1157, https://doi.org/10.1130/GES01133.1.

Ratschbacher, B.C., Keller, C.B., Schoene, B., Paterson, S.R., Anderson, J.L., Okaya, D., Putirka, K., and Lippoldt, R., 2018, A new workflow to assess emplacement duration and melt residence time of compositionally diverse magmas emplaced in a sub-volcanic reservoir: Journal of Petrology, v. 59, p. 1787–1809, https://doi.org/10.1093/petrology/egy079.

Rioux, M., Lissenberg, C.J., McLean, N.M., Bowring, S.A., MacLeod, C.J., Hellebrand, E., and Shimizu, N., 2012, Protracted timescales of lower crustal growth at the fast-spreading East Pacific Rise: Nature Geoscience, v. 5, p. 275–278, https://doi.org/10.1038/ngeo1378.

Rioux, M., Farmer, G.L., Bowring, S.A., Wooton, K.M., Amato, J.M., Coleman, D.S., and Verplanck, P.L., 2016, The link between volcanism and plutonism in epizonal magma systems: High-precision U-Pb zircon geochronology from the Organ Mountains caldera and batholith, New Mexico: Contributions to Mineralogy and Petrology, v. 171, p. 13, https://doi.org/10.1007/s00410-015-1208-6.

Samperton, K.M., Schoene, B., Cottle, J.M., Keller, C.B., Crowley, J.L., and Schmitz, M.D., 2015, Magma emplacement, differentiation, and cooling in the middle crust: Integrated zircon geochronological-geochemical constraints from the Bergell Intrusion, Central Alps: Chemical Geology, v. 417, p. 322–340, https://doi.org/10.1016/j.chemgeo.2015.10.024.

Samperton, K.M., Bell, E.A., Barboni, M., Keller, C.B., and Schoene, B., 2017, Zircon age-temperature-compositional spectra in plutonic rocks: Geology, v. 45, p. 983–986, https://doi.org/10.1130/G38645.1.

Schaen, A.J., Cottle, J.M., Singer, B.S., Keller, C.B., Garibaldi, N., and Schoene, B., 2017, Complementary crystal accumulation and rhyolite melt segregation in a late Miocene Andean pluton: Geology, v. 45, p. 835–838, https://doi.org/10.1130/G39167.1.

Schaen, A.J., Schoene, B., Dufek, J., Singer, B.S., Eddy, M.P., Jicha, B.R., and Cottle, J.M., 2021, Transient rhyolite melt extraction to produce a shallow granitic pluton: Science Advances, v. 7, no. 21, eabf0604, https://doi.org/10.1126/sciadv.abf0604.

Schoene, B., Latkoczy, C., Schaltegger, U., and Günther, D., 2010, A new method integrating high-precision U-Pb geochronology with zircon trace element analysis (U-Pb TIMS-TEA): Geochimica et Cosmochimica Acta, v. 74, p. 7144–7159, https://doi.org/10.1016/j.gca.2010.09.016.

Schoene, B., Schaltegger, U., Brack, P., Latkoczy, C., Stracke, A., and Günther, D., 2012, Rates of magma differentiation and emplacement in a ballooning pluton recorded by U-Pb TIMS-TEA, Adamello batholith, Italy: Earth and Planetary Science Letters, v. 335–356, p. 162–173, https://doi.org/10.1016/j.epsl.2012.08.019.

Schoene, B., Barboni, M., and Samperton, K.M., 2015, U-Pb Geochronology: Taking or creating the pulse of magmatic systems?: San Francisco, California, American Geophysical Union, Abstract T31F-2910 presented at 2015 Fall Meeting, 14–18 December.

Schoene, B., Eddy, M.P., Samperton, K.M., Keller, C.B., Keller, G., Adatte, T., and Khadri, S.F.R., 2019, U-Pb constraints on pulsed eruption of the Deccan Traps across the end-Cretaceous mass extinction: Science, v. 363, p. 862–866, https://doi.org/10.1126/science.aau2422.

Shaw, H.R., 1965, Comments on viscosity, crystal settling, and convection in granitic magmas: American Journal of Science, v. 263, p. 120–152, https://doi.org/10.2475/ajs.263.2.120.

Shea, E.K., Miller, J.S., Miller, R.B., Bowring, S.A., and Sullivan, K.M., 2016, Growth and maturation of a mid- to shallow-crustal intrusive complex, North Cascades, Washington: Geosphere, v. 12, no. 5, p. 1489–1516, https://doi.org/10.1130/GES01290.1.

Sisson, T.W., and Bacon, C.R., 1999, Gas-driven filter pressing in magmas: Geology, v. 27, no. 7, p. 613–616, https://doi.org/10.1130/0091-7613(1999)027<0613:GDFPIM>2.3.CO;2.

Sláma, J., Košler, J., Condon, D.J., Crowley, J.L., Gerdes, A., Hanchard, J.M., Horstwood, M.S.A., Morris, G.A., Nasdala, L., Norberg, N., Schaltegger, U., Schoene, B., Tubrett, M.N., and Whitehouse, M.J., 2008, Plešovice zircon—A new natural reference material for U-Pb and Hf isotopic microanalysis: Chemical Geology, v. 249, p. 1–35, https://doi.org/10.1016/j.chemgeo.2007.11.005.

Tappa, M.J., Coleman, D.S., Mills, R.D., and Samperton, K.M., 2011, The plutonic record of a silicic ignimbrite from the Latir volcanic field, New Mexico: Geochemistry, Geophysics, Geosystems, v. 12, Q10011, https://doi.org/10.1029/2011GC003700.

Tavazzani, L., Peres, S., Sinigoi, S., Demarchi, G., Economos, R.C., and Quick, J.E., 2020, Rejuvenation and melt extraction recorded in Permian plutonic and volcanic rocks of the Sesia Magmatic System (Southern Alps, Italy): Journal of Petrology, v. 61, egaa049, https://doi.org/10.1093/petrology/egaa049.

Tuttle, O.F., and Bowen, N.L., 1958, Origin of granite in the light of experimental studies in the system $NaAlSi_3O_8$-$KAlSi_3O_8$-SiO_2-H_2O: Geological Society of America Memoir 74, 153 p., https://doi.org/10.1130/MEM74.

Vigneresse, J.L., Barbey, P., and Cuney, M., 1996, Rheological transitions during partial melting and crystallization with application to felsic magma segregation and transfer: Journal of Petrology, v. 37, p. 1579–1600, https://doi.org/10.1093/petrology/37.6.1579.

Walker, B.A., Jr., Miller, C.F., Claiborne, L.L., Wooden, J.L., and Miller, J.S., 2007, Geology and geochronology of the Spirit Mountain batholith southern Nevada: Implications for timescales and physical processes of batholith construction: Journal of Volcanology and Geothermal Research, v. 167, p. 239–262, https://doi.org/10.1016/j.jvolgeores.2006.12.008.

Wiedenbeck, M., Hanchar, J.M., Peck, W.H., Sylvester, P., Valley, J., Whitehouse, M., Kronz, A., Morishita, Y., Nasdala, L., Fiebig, J., Franchi, I., Girard, J.P., Greenwood, R.C., Hinton, R., Kita, N., Mason, P.R.D., Norman, M., Ogasawara, M., Piccoli, P.M., Rhede, D., Satoh, H., Schulz-Dobrick, B., Skår, O., Spicuzza, M.J., Terada, K., Tindle, A., Togashi, S., Vennemann, T., Xie, Q., and Zheng, Y.F., 2004, Further characterization of the 91500 zircon crystal: Geostandards and Geoanalytical Research, v. 28, p. 9–39, https://doi.org/10.1111/j.1751-908X.2004.tb01041.x.

Wotzlaw, J.F., Schaltegger, U., Frick, D.A., Dungan, M.A., Gerdes, A., and Günther, D., 2013, Tracking the evolution of large-volume silicic magma reservoirs from assembly to supereruption: Geology, v. 41, p. 867–870, https://doi.org/10.1130/G34366.1.

Zuza, A.V., Cao, W., Hinz, N.H., DesOrmeau, J.W., Odlum, M.L., and Stockli, D.F., 2019, Footwall rotation in a regional detachment fault system: Evidence for horizontal-axis rotational flow in the Miocene Searchlight pluton, NV: Tectonics, v. 38, p. 2506–2539, https://doi.org/10.1029/2019TC005513.